METHODOLOGIES FOR CAVITY PREDICTION BASED ON ANALYSIS OF SURFACE TEMPERATURE DISTRIBUTIONS

BY

KUO CHIN SU

A DISSERTATION PRESENTED TO THE GRADUATE COUNCIL OF
THE UNIVERSITY OF FLORIDA
IN PARTIAL FULFILLMENT OF THE REQUIREMENTS FOR THE
DEGREE OF DOCTOR OF PHILOSOPHY

UNIVERSITY OF FLORIDA

1979

To My Parents

ACKNOWLEDGEMENTS

The author wishes to express his sincere appreciation to his graduate supervisory committee which included Dr. C.K.Hsieh, chairman; Dr. R.K.Irey; Dr. R.A.Gater; Dr. H.A.Ingley,III; and, Dr. C.Luehr. Special thanks go to his advisor, Dr. C.K.Hsieh, without whose excellent guidance and helpful advice this work would not have been possible.

The author also wishes to thank his wife, Jew Whei. Her patience and encourgement made his five years of graduate study a beautiful memory.

Finally, the author wishes to acknowledge the National Science Foundation (Grant No. ENG-7710630) for financial support for this work.

TABLE OF CONTENTS

		Page
ACKNOWLEDGEMENTS		iii
LIST OF TABLES		vii
LIST OF FIGURES		viii
KEY TO SYMBOLS		x
ABSTRACT		xiii
CHAPTER		
I	INTRODUCTION	1
II	PROBLEM 1: BOUNDARY CONDITION OF THE FIRST KIND AT THE CAVITY SIDE	6
	Analysis	9
	Error Analysis	9
	Example and Discussion	15
	Extension to Two Dimensional Systems	22
III	PROBLEM 2: BOUNDARY CONDITION OF THE SECOND KIND AT THE CAVITY SIDE	26
	Analysis	27
	Example and Discussion	34
	Extension to Two Dimensional Systems	38
IV	PROBLEM 3: BOUNDARY CONDITION OF THE THIRD KIND AT THE CAVITY SIDE	44
	Pattern Recognition Theory	44
	Example and Discussion	46

Page

V CONCLUSIONS..... 56

VI RECOMMENDATIONS..... 58

APPENDICES:

APPENDIX A A SUPERPOSITION SOLUTION OF HEAT CONDUCTION IN A CAVITIED REGION SUBJECTED TO A CONVECTIVE BOUNDARY CONDITION..... 61

Introduction..... 61

Analysis..... 63

Critique..... 71

Results and Discussion..... 74

APPENDIX B COMPUTER PROGRAM FOR COMPUTATION OF SURFACE TEMPERATURES ON A PLANE WALL HAVING A PRESCRIBED CAVITY GEOMETRY, THE LOWER BOUNDARY HAVING A SPECIFIED TEMPERATURE..... 80

APPENDIX C COMPUTER PROGRAM TO PREDICT CAVITY GEOMETRY FOR THE SYSTEM GIVEN IN APPENDIX B..... 87

APPENDIX D COMPUTER PROGRAM FOR COMPUTATION OF SURFACE TEMPERATURES FOR A RECTANGULAR PARALLELEPIPED WITH A PRESCRIBED RECTANGULAR HOLE IN IT, THE HOLE BOUNDARY HAVING A SPECIFIED TEMPERATURE... 93

APPENDIX E COMPUTER PROGRAM TO PREDICT CAVITY GEOMETRY FOR THE SYSTEM GIVEN IN APPENDIX D..... 99

APPENDIX F COMPUTER PROGRAM FOR COMPUTATION OF SURFACE TEMPERATURES ON A PLANE WALL HAVING A PRESCRIBED CAVITY GEOMETRY, THE LOWER BOUNDARY SUBJECTED TO A CONSTANT HEAT FLUX..... 106

APPENDIX G COMPUTER PROGRAM TO PREDICT CAVITY GEOMETRY FOR THE SYSTEM GIVEN IN APPENDIX F..... 113

APPENDIX H COMPUTER PROGRAM FOR COMPUTATION OF SURFACE TEMPERATURES FOR A RECTANGULAR PARALLELEPIPED WITH A PRESCRIBED RECTANGULAR HOLE IN IT, THE HOLE BOUNDARY SUBJECTED TO A CONSTANT HEAT FLUX..... 119

APPENDIX I COMPUTER PROGRAM FOR COMPUTATION OF SURFACE TEMPERATURES ON A PLANE WALL HAVING A PRESCRIBED CAVITY GEOMETRY, THE LOWER BOUNDARY SUBJECTED TO A CONVECTIVE CONDITION... 127

Page

REFERENCES 135

BIOGRAPHICAL SKETCH 138

LIST OF TABLES

Table		Page
1	Input Data for a Numerical Solution of Surface Temperatures for a Problem Having a Boundary Condition of the Third Kind at the Cavity Side	47
2	Comparison Between Predicted and Analyzed s for Systems Having Rectangular Cavities	77
3	Definitions of Input Variables for the Program Given in Appendix B	80
4	Definitions of Additional Input Variables for the Program Given in Appendix C	87
5	Definitions of Input Variables for the Program Given in Appendix D	93
6	Definitions of Input Variables for the Program Given in Appendix E	99
7	Definitions of Input Variables for the Program Given in Appendix F	106
8	Definitions of Input Variables for the Program Given in Appendix G	113
9	Definitions of Input Variables for the Program Given in Appendix H	119
10	Definitions of Input Variables for the Program Given in Appendix I	127

LIST OF FIGURES

Figure		Page
1	Schematic of a Basic System Under Investigation	4
2	Nodal Points Lay-out	7
3	Chart of Error Propagation due to $h(\Delta y)/k$ Uncertainty	12
4	Chart of Error Propagation due to Surface Temperature Uncertainty	14
5	Use of Surface Temperatures to Predict Cavity Geometry in Problem 1	16
6	Recheck of Cavity Wall Position in Problem 1	20
7	Flow Diagram Showing Procedures to Evaluate Cavity Geometry in Problem 1	23
8	Prediction of Hole Geometry in a Parallelepiped in Problem 1	25
9	Illustration of a Superposition Technique	28
10	Use of Surface Temperatures to Predict Cavity Geometry in Problem 2	35
11	Recheck of Cavity Wall Position in Problem 2	36
12	Flow Diagram Showing Procedures to Evaluate Cavity Geometry in Problem 2	39
13	Partition of Hole into Four Quadrants in a Two-dimensional Analysis	40
14	Prediction of Hole Geometry in a Parallelepiped in Problem 2	43
15	Sample Output of a Surface Temperature Pattern in Problem 3	49
16	A Plot of Inflection Point Location Versus Cavity Width and Depth in Problem 3	50

Figure		Page
17	A Plot of Peak Surface Temperature Versus Cavity Depth and Width in Problem 3	51
18	A Plot of Edge Surface Temperature Versus Cavity Depth in Problem 3	52
19	Flow Diagram Showing Procedures to Evaluate Cavity Geometry Using Correlation Equations	55
20	Systems for Analysis	64
21	Notations for Cavities	68
22	Comparison Between the True and Predicted Temperatures Based on an Approximate Solution	75
23	Correlation Between Predicted and Analyzed s	78
24	A Schematic Diagram Showing Nodal Locations Used in the Computer Program Given in Appendix B	81
25	Block Diagram Showing Iteration Procedures for the Computer Program Given in Appendix B	82
26	Block Diagram for the Computer Program Given in Appendix C	88
27	A Schematic Diagram Showing Nodal Locations Used in the Computer Program for a Parallelepiped	94
28	Block Diagram Showing Iteration Procedures for the Computer Program Given in Appendix D	95
29	Block Diagram for the Computer Program Given in Appendix E	100
30	Block Diagram for the Computer Program Given in Appendix F	107
31	Block Diagram for the Computer Program Given in Appendix G	114
32	Block Diagram for the Computer Program Given in Appendix H	120
33	Block Diagram for the Computer Program Given in Appendix I	128

KEY TO SYMBOLS

A_c	Area of the cavity
a	Major axis of the elliptical cavity
Bi	= hL/k
$Bi_{(\ell-s)}$	= h(ℓ-s)/k
b	Minor axis of the elliptical cavity
C_n	= equation (22)
D	$=[(\Delta y)/(\Delta x)]^2$
d	Depth of the rectangular cavity
E_n	a constant
e	error
f	heat flux or a function
G	= equation (20)
g	crossflow heat flux
h	convective coefficient
I,J	index in x, y directions, respectively
k	thermal conductivity
L	length of system in x direction; $[1+D+h(\Delta y)/k]e_T$
ℓ	Thickness of system in y direction
M	Upper limit of index I
N	Upper limit of index J

n	$=1,2,3,\ldots.$
Nu	Nusselt number
P	$= -De_T/2$
Q	Total heat flow per unit depth of system
r_o	Radius of the circular cavity
Re	Reynolds number
S	$= 1+D$
s	Shift of x-axis
T	Temperature or true temperature
T_b	Surface temperature (a prescribed boundary condition)
T_∞	Ambient temperature
U	$=[T(x,y)-T_A]/T_A$
u	Opening width of the triangular cavity
V	Computed temperature
v	Depth of the triangular cavity
W	$=W(\xi,\eta)$
w	Width of the rectangular cavity
x,y	Independent variables or coordinates
y_o	$f(x)$, function for lower boundary contour
Z	$=Z(\xi,\eta)$
α	$=a/(\ell-s)$
β	$=b/(\ell-s)$
γ	$=L/(\ell-s)$
δ	$=d/L$ or $d/(\ell-s)$
ϵ	Convergence criterion or a perturbation parameter

η	$=y/L$
η_o	$=f(\xi)$, normalized function for lower boundary contour
θ	$=[T(x,y)-T_\infty]/(T_b-T_\infty)$
θ_o	First part of the superimposed solution
θ_1	Second part of the superimposed solution
λ_m,λ_n	Eigenvalues
μ	$=\ell/L$ or $u/(\ell-s)$
ν	Dummy variable of integration; $v/(\ell-s)$
ξ	$=x/L$ or $x/(\ell-s)$
ρ	$=r_o/(\ell-s)$
σ	$=s/(\ell-s)$
ω	$=w/L$ or $w/(\ell-s)$

Subscripts

A	Refer to ambient
a	Refer to ambient of the lower boundary in problem 3
B	Refer to boundary or $h(\Delta y)/k$
S	Refer to surface
T	Refer to temperature
t	Refer to total
1,2	Refer to regions
I,II,III, IV	Refer to quadrants

Prefix

Δ	Mesh size of what follows
∇^2	Laplacian

Abstract of Dissertation Presented to the Graduate Council
of the University of Florida in Partial Fulfillment of the
Requirements for the Degree of Doctor of Philosophy

METHODOLOGIES FOR CAVITY PREDICTION BASED ON ANALYSIS
OF SURFACE TEMPERATURE DISTRIBUTIONS

By

Kuo Chin Su

August, 1979

Chairman: C.K. Hsieh
Major Department: Mechanical Engineering

The scanned surface temperature data from a body is used to predict the cavity lying underneath the surface. The basic system under investigation is a plane wall having a rectangular cavity at the back surface. The front surface dissipates heat by convection; this is also the surface whose temperature is scanned. Three types of boundary conditions are considered on the back surface. For a prescribed surface temperature specified on the cavity side, a numerical solution is found convenient to predict the cavity top and the approximate location of the cavity wall. A recheck of the cavity wall position calls for matching the recalculated surface temperature with the measured temperature. The data are found to be well behaved to the extent that an interpolation is possible when the mesh size chosen happens to miss the wall position.

In the second problem, the heat flux at the cavity side is given. Using this heat flux the cavity depth can be determined. An exact solution is found convenient for this case to check the cavity wall position. The method used is to divide the system about the cavity into two regions and use the additional surface temperature observed above the cavity top to

find a cross heat flux between the divided regions. In this way the surface temperature on the remaining boundary can be recalculated and used to match the measured temperature.

For a convective condition appearing on the cavity side, neither of the aforementioned methods works. A pattern recognition method using the common-property approach is found useful to predict the cavity in this instance.

The methodologies developed for the first two types of problems (prescribed temperature or heat flux at the cavity side) are also extended to predict holes in a parallelepiped. In contrast to what one might expect, because of additional surface temperatures available for this system, the prediction method turns out to be less sophisticated. Certainties can be raised for all instances provided that the thermal conductivity and the convective coefficient values used in the prediction are correct.

CHAPTER I

INTRODUCTION

In the classical problem of heat conduction, the system configuration has to be specified. The governing equation can be formulated based on the physics of the problem. Then, if the boundary conditions are given, a solution can be effected to determine the temperature distribution at each point interior to the system. There is another type of problem in which either the temperature, or the temperature-time history is given at some interior points, and it is desirable to find either the surface temperature or the surface heat flux at boundaries. This latter type of problem is often termed the inverse problem and is encountered in quenching process, calorimetry and convection studies, among others [1-7]. Of little investigation in the heat transfer literature is a third type of problem which, although also related to the inverse problem, serves a totally different purpose. In this third type of problem, the system has an unknown configuration and one of the system boundaries has an additional measurable temperature in addition to a convective condition (boundary condition of the third kind) that is imposed on this surface. The purpose of the problem is to determine the configuration of the boundary opposite to this surface [8-13].

The third type of problem has received interest only recently when, in nondestructive testings using infrared scanning, one can scan the surface temperature of a body that dissipates heat by convection (including radiation) to the surroundings. The inner boundary is subjected to varied

boundary conditions, and the purpose of performing infrared scanning is to determine the cavity, if any, at the inner boundary. The problem is, in fact, of contemporary interest. With the development of the Computerized Axial Tomography (CAT), the infrared scanning carries promise of being a viable alternative to the x-ray scanning [14-18].

It should be noted that, while both the CAT and the infrared scanning can be used to map the interior of a body, their mechanisms of operation are different. The CAT operates on the extinction characteristics of the material; with the body tissues made of primarily radiation absorbers, classical methods such as matrix inversions and the Fourier transforms of images are useful to reestablish images of nonhomogenity in the medium [19]. In contrast, the infrared scanning method monitors the surface radiosity as a function of the diffusion of heat in the medium. With the transverse coupling in heat diffusion that is as important as the longitudinal heat propagation, the heat penetrated in the medium in more than one direction. Hence, the infrared image cannot be analyzed in the same way as those used in the analysis of CAT images. This dissimilarity makes the problem a real challenge to investigators.

It is worth noting that, while the inverse problem as stated appears to be well known in the field of nondestructive testing, an exact solution of the problem has not been found in the literature. Indeed, an analytical solution of problems having irregular boundaries subjected to a convective boundary condition defies an exact solution* by either a conformal mapping or a Schwarz-Christoffel transformation. Numerical methods such as the

*An approximate solution has been developed and presented in Appendix A.

Schwarz iteration technique are also handicapped because of the appearance of a convective condition at the surface. The problem as stated can, of course, be solved numerically using a finite difference or a finite element method in conjunction with an iteration scheme or a matrix inversion. This requires the presumption of a cavity to yield a surface temperature in order to match the observed temperature. Such a gross trial and error solution falls within the category of template matching schemes in the pattern recognition process [20]. The method, although functional, [8-10, 21,22], is time consuming from the computation standpoint and, therefore, is of no concern to us in this study.

In this dissertation three different techniques will be presented with each one devised to solve a certain type of boundary condition at the cavity side. To facilitate presentation, materials that are relevant to one test method are compiled and presented in one chapter of the dissertation. This includes the analysis, working examples and error analysis, if necessary. In all instances, the basic system under investigation consists of a plane wall having a rectangular cavity on the bottom surface, see Fig. 1. The top surface dissipates heat by convection (including radiation through a suitable h). This is also the surface whose temperature is monitored by an infrared scanner and, therefore, this temperature is known. The left and right edges of the system are insulated. Physically, these edges simulate sections remote from the cavity where the temperature gradients are negligible. On the bottom boundary three different conditions are considered that include the prescribed surface temperature, the prescribed heat flux and the convective condition (i.e., boundary condition of the first kind, second kind and third kind.

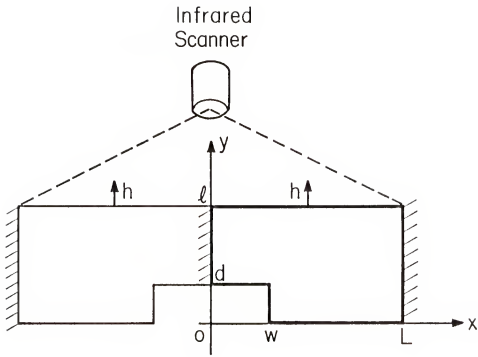

Figure 1

Schematic of a Basic System Under Investigation

respectively). They represent three different types of problems and call for three different methods of solution.

For the system under investigation, because of temperature symmetry, only one half of the system is needed for analysis. It is further assumed that the system is in steady state. Variations of temperatures in z direction (perpendicular to the plane of Fig. 1), as well as the thermophysical properties with temperatures, are ignored.

CHAPTER II

PROBLEM 1: BOUNDARY CONDITION OF THE FIRST KIND AT THE CAVITY SIDE

For a specified temperature T_B imposed on the cavity side of the boundary, the problem is simplified by the fact that the boundary temperature at the top surface can be used as a clue to identify the cavity geometry. It has been noted earlier that the top surface dissipates heat by convection to the surroundings and the top surface temperature is also measured. This permits the use of the surface temperature and the ambient temperature to determine the nodal temperatures inside the system; see Fig. 2. The computation commences with the first row of interior nodes right underneath the top surface. The nodal temperatures are calculated one row after another in a downward direction until one (or more) temperatures in one row of nodes reach (or exceed) the prescribed level (T_B). If the nodal temperature calculated at one point exceeds the boundary temperature, this point must be lying inside the cavity region. Then, an interpolation scheme must be used to determine the cavity location.

A further continuation of computation downward will evaluate nodal temperatures inside the cavity region. While these temperatures have no bearing on the determination of the cavity top position, these temperatures will upset data near the cavity (side) wall. This point can be better illustrated by reference to Fig. 2. Say, the cavity is located $1 \leq I \leq 5$ and $1 \leq J \leq 3$ and the mesh size chosen is good, then the computation yields acceptable data up to row J = 3 inclusive. Proceeding further downward will yield temperatures at nodes (1 to 5,2) higher than the prescribed.

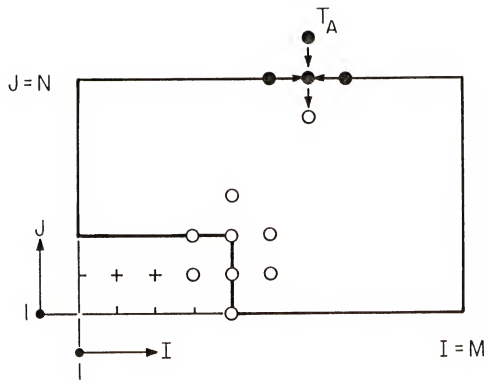

Figure 2

Nodal Points Lay-out

Particularly, the high temperature at node (5,2) will raise the temperature at node (5,1) above the prescribed level. As a result, the prediction of the corner location will be in error. It is also noted that, since it takes four nodes above a given point to predict the nodal temperature in question, the overprediction of temperatures for corner nodes will not be affected whether the computation of temperatures is from left to right or right to left.

For the rectangular cavity addressed in this study, one would be inclined to say that the predicted nodal temperatures at row J=3 (still use the previous example) should give sufficient indication as to where the cavity wall is located. Unfortunately, this is not so. Because of the rapid propagation of numerical errors (to be examined later), a data smooth routine must be employed. As such, the temperature calculated at the cavity reentrant corner will not be precisely at the prescribed level. While the approximate location of this corner can be identified based on the calculated nodal temperatures, its actual location must still be verified. This can be done by picking a cavity wall position and resolve the problem, this time for a top surface temperature. If this calculated temperature matches the initially measured one, the assumed wall location is correct. A small trial and error is still needed. But, since the cavity top position has been identified, and the approximate position of the cavity wall is also known, the time involved in the trial and error can be greatly curtailed. An example will be provided later to illustrate these points.

Analysis

The analysis is facilitated by reference to Fig. 2. For the system shown, under a steady state condition, only two general nodal equations are needed to calculate the interior nodal temperatures. For nodes in row J=N-1,

$$T_{I,N-1} = \frac{(\Delta y)}{(\Delta x)} \left\{ \left[\frac{h(\Delta x)}{k} + \frac{(\Delta y)}{(\Delta x)} + \frac{(\Delta x)}{(\Delta y)} \right] T_{I,N} - \frac{h(\Delta x)}{k} T_A \right.$$

$$\left. - \frac{(\Delta y)}{2(\Delta x)} (T_{I+1,N} + T_{I-1,N}) \right\} \qquad (1)$$

For nodes in rows $J \leq (N-2)$,

$$T_{I,J} = \frac{(\Delta y)}{(\Delta x)} \left\{ 2 \left[\frac{(\Delta y)}{(\Delta x)} + \frac{(\Delta x)}{(\Delta y)} \right] T_{I,J+1} - \frac{(\Delta x)}{(\Delta y)} T_{I,J+2} \right.$$

$$\left. - \frac{(\Delta y)}{(\Delta x)} (T_{I-1,J+1} + T_{I+1,J+1}) \right\} \qquad (2)$$

where (Δx) and (Δy) are mesh sizes in x and y directions, respectively. h is the convective heat transfer coefficient; k, the thermal conductivity; T_A, the ambient temperature. Since both T_A and $T_{I,N}$ are known, the numerical solution is self starting. The above two equations can also be rearranged to solve for interior nodal temperatures when the problem is reworked to find the top surface temperature.

Error Analysis

Since the nodal temperatures are used as a vehicle to determine the cavity boundary, the accuracy of the prediction relies heavily on the accuracy of the nodal temperatures that can be calculated in the analysis. Among those parameters that have a bearing on the results the thermal conductivity and the convective heat transfer coefficient are important. The

thermal conductivity can be measured with an accuracy of 1.5 to 3%, depending on the method used, according to the current state of the art [23]. The uncertainty in the convective coefficient is usually larger. However, since these two parameters always appear together in the equation (see equation (1)), it is convenient to consider the error of the dimensionless group $h(\Delta y)/k$ as presented below.

If the actual $h(\Delta y)/k$ value used in the analysis is off by a dimensionless quantity e_B and all the temperatures are evaluated in excess of T_A, then the difference between the actual computed temperature V and the true temperature T for nodes in row (N-1) can be derived using equation (1) and expressed in terms of $T_{I,N}$ as,

$$V_{I,N-1} - T_{I,N-1} = e_B T_{I,N} \tag{3}$$

This error will propagate to nodes (I,N-2) and causes errors there, given as,

$$V_{I,N-2} - T_{I,N-2} = 2e_B S\, T_{I,N} - e_B D(T_{I-1,N} + T_{I+1,N}) \tag{4}$$

where,

$$D = \left[\frac{(\Delta y)}{(\Delta x)} \right]^2, \quad S = 1+D$$

The errors at nodes (I,N-3) become more complicated and can again be expressed in terms of the surface temperatures as,

$$V_{I,N-3} - T_{I,N-3} = e_B(4S^2+2D^2-1)T_{I,N} - 4e_B SD(T_{I-1,N}+T_{I+1,N})$$

$$+e_B D^2(T_{I-2,N}+T_{I+2,N}) \tag{5}$$

By comparing these three equations, a pattern of error propagation can be found as depicted in Fig. 3. At the top of the figure a set of coefficient multipliers is given in a boxed chart. This chart can be used to develop coefficients for T on the right of equations (4) and (5) as follows. Using equation (3), one obtains the coefficient for $T_{I,N}$ term as e_B, see row (N-1) in the figure. Using this e_B and the multiplier chart, one finds the coefficients for $T_{I,N}$, $T_{I-1,N}$ (or $T_{I+1,N}$) terms in equation (4) as $2e_BS$ ($=e_B \times 2S$), $-e_BD(=e_B \times (-D))$, respectively. Somewhat peculiar is the presence of $(-e_B)$ in column I in the tabulation for (N-3) row. This additional coefficient arises from the fact that, in the formulation of the temperature equation for row (N-3), terms of temperature for row (N-1) also enter into the equation. By the same token, if one derives the equation for $(V_{I,N-4}-T_{I,N-4})$, those coefficients contained in row (N-2) will also appear in the equation (not shown) and, therefore, be subtracted from the $T_{I-1,N}$, $T_{I,N}$ and $T_{I+I,N}$ terms. It is noted that in the foregoing analysis, the errors in the interior nodal temperatures have all been expressed in terms of the surface temperatures; see equations (3), (4) and (5). Also the examples given here have been made based on the propagation of errors from temperatures at points (I,N-1).

Another error arises from the surface temperature uncertainty. The surface temperature measured using an infrared scanner is susceptible to errors due to surface irregularities such as rough spots, rusts, etc. Hence, an error analysis is also needed to examine how a singular surface temperature irregularity could affect the temperatures at interior nodes.

If the true temperature at point (I,N) is denoted as $T_{I,N}$ and the observed value there is $T_{I,N}(1+e_T)$, the error at the point can be represented by $e_T T_{I,N}$ where e_T denotes the percent error in T value. One can

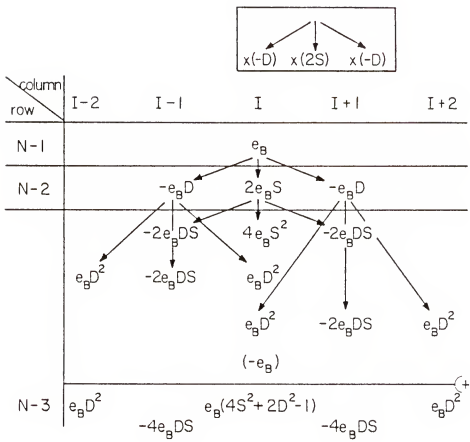

Figure 3

Chart of Error Propagation due to $h(\Delta y)/k$ Uncertainty

use equation (1) to prove that the difference between the computed temperature V and the true temperature T at point (I,N-1) due to the singular temperature uncertainty at point (I,N) is,

$$V_{I,N-1} - T_{I,N-1} = LT_{I,N} \tag{6}$$

where,

$$L = \left[1 + D + \frac{h(\Delta y)}{k} \right] e_T$$

The uncertainty at point (I+1,N-1) can also be derived and expressed in terms of the surface temperature as,

$$V_{I+1,N-1} - T_{I+1,N-1} = PT_{I,N} \tag{7}$$

where,

$$P = -(1/2)De_T$$

The multiplier chart given in Fig. 3 is again useful to derive the temperature error equations for nodes deep inside the system. For example, at point (I,N-2),

$$V_{I,N-2} - T_{I,N-2} = (2SL - 2DP - e_T)T_{I,N} \tag{8}$$

which can be obtained from the multiplication table given in Fig. 4.

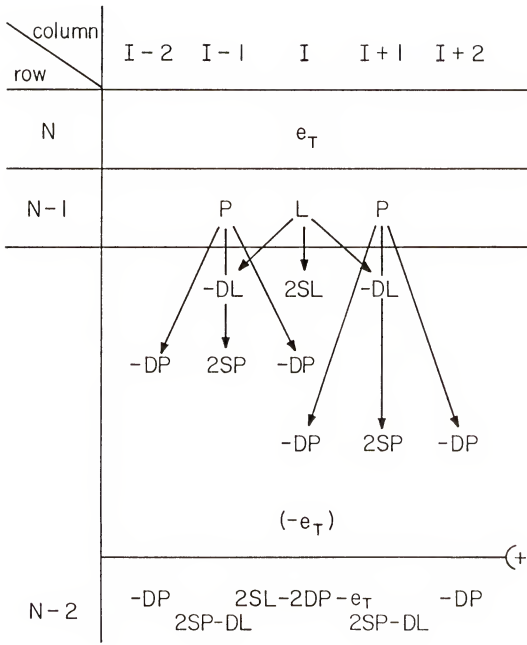

Figure 4

Chart of Error Propagation due to Surface Temperature Uncertainty

Example and Discussion

A series of tests was made to validate the methodology presented in this chapter. The top surface temperatures were calculated for test cases having known cavity geometries. The method used in the calculation was an iteration scheme that was commonly employed in the numerical solution of heat conduction problems.* These surface temperatures calculated were subsequently used as inputs to a computer program to solve inversely the nodal temperatures underneath the surface which, in turn, were used to reconstruct the cavity configuration. A sample test is shown in Fig. 5 where the test parameters are listed in the legend.

Attention is first directed to the calculated surface temperature appearing on the top of the figure. Because of the presence of the cavity the surface has a hot spot above the cavity, which is not unexpected. It is noted that the inflection point on the temperature data does not coincide with the location of the cavity (side) wall; this point is always displaced away from the cavity center. This phenomenon can be ascribed to the fact that additional heat flux is needed to maintain the cavity wall at a prescribed temperature. This additional flux crosses the system boundary and raises the temperatures near the wall.

The calculated surface temperature was next used in an inverse problem to predict the cavity geometry.+ In the middle diagram a cross section of the analyzed system is shown, where the solid line at lower

*The computer program useful for this part of the work is presented in Appendix B.

+ A computer program to solve this inverse problem is included in Appendix C.

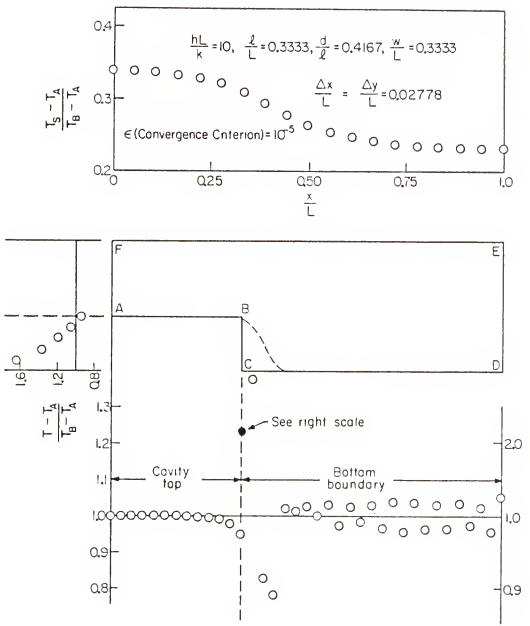

Figure 5

Use of Surface Temperatures to Predict Cavity Geometry in Problem 1

left corner depicts the actual cavity location. If the interior nodal temperatures are calculated one row after another covering the entire region and, if the isotherm at T_B (prescribed) is plotted in the figure, the dashed line is obtained. Clearly, this scheme of predicting the cavity geometry yields acceptable results at the cavity top, but the cavity reentrant corner is in error and the width of the cavity base is also overpredicted. To facilitate viewing of the disagreement between the predicted nodal temperature and the prescribed temperature (T_B) along the cavity boundary, two additional temperature plots are given as shown in the bottom and left of the figure. The bottom figure compares the calculated nodal temperatures with T_B along the cavity top (AB) and the bottom boundary (CD); the left figure makes a similar comparison for the cavity wall (BC). As shown in the bottom figure, start from point A, the prediction of the cavity top is indeed accurate (agreement within 0.1%). Toward the cavity reentrant corner (B), the calculated nodal temperatures are slightly lower; see both bottom and left figures; note different scales used in these plots. Moving down along the cavity wall (BC), the calculated nodal temperatures increase rapidly; see left figure. Of particular interest is the observation of temperature oscillations along the bottom boundary (CD); see the bottom figure. This demonstrates the characteristics of the numerical method used in the solution. Since the nodal temperature at any point is calculated based on those at four nodes right above the point (see Fig. 2), a minute temperature fluctuation at the node right above the point of investigation tends to amplify rapidly downward and affect those temperatures calculated below the fluctuating point. Unlike the conventional solution by iteration method, in which the nodal temperatures at a point

are calculated based on those temperatures at their immediate vicinity and, as such, for successive computations, any temperature fluctuations tend to damp out, the numerical method used in the present study computes temperatures one row after another in a fixed direction. Hence, any temperature fluctuation at a point will not damp out but will amplify and show markedly in a succeeding row at the same column position. This problem must be resolved and the method found successful was to apply a noise removal routine as what was commonly used in the field of image processing [20,22]. According to the method, a moving average of temperatures is computed using,

$$T_{I,J(\text{smoothed})} = \frac{T_{I-1,J}+6T_{I,J}+T_{I+1,J}}{8} \tag{9}$$

which was derived based on averaging $T_{I,J}$ with $T_{I-1,J}$ (or $T_{I+1,J}$) to get the first pair of means, which are, in turn, added to $T_{I,J}$ itself to compute a second set of means. Equation (9) computes the third order mean value based on the previously calculated means. Clearly, this equation provides sufficient weight to the original $T_{I,J}$ data to retain its characteristics while producing a desired smoothing function satisfactory for a wide range of cases including small mesh size and shallow cavities. It is also noted that, since the slope of the surface temperature near the cavity center is negligibly small, this data smoothing routine will not affect the determination of the position of the cavity top. However, the nodal temperatures calculated near the cavity (side) wall are somewhat smeared to the extent that the exact position of the cavity reentrant corner cannot be identified based on the computed nodal temperatures. This also explains why the calculated nodal temperature at the cavity

reentrant corner is slightly lower than prescribed; refer to Fig. 5. A recheck of the corner position is in order.

Based on the foregoing analysis, a cavity wall position can be assumed. Experience suggests that the cavity reentrant corner should be located beyond the point where the nodal temperatures show a trend of dropping. With this assumed cavity wall, temperatures inside and on the surface of the system are recalculated and the latter plotted as shown in Fig. 6.

If the assumed wall position is one mesh size (Δx) smaller than the actual width (i.e., cavity width underpredicted), the recalculated surface temperature T_S is lower than the measured as is shown in the lower half of the figure. An overprediction by one mesh size moves the data to the top. The solid line across the figure represents where data are located when the prediction is correct. Moreover, the data located in the top half of the figure appears to form a mirror image below the solid line, signifying that an interpolation is again possible in the searching process. According to the trend of data shown the interpolation appears to be most effective near the temperature inflection point where the data vary most rapidly.

With the discussion of the prediction of cavity geometry complete, attention is now directed to the error analysis. Tests were made with the $h(\Delta y)/k$ value overestimated 5%. For this case, the computer data reveal that the predicted cavity is 6.5% deeper. A value of $h(\Delta y)/k$ 5% lower will lead to a prediction of cavity depth 7.4% shallower. On the other hand, because of the method of numerical solution used in this work, any erroneous temperature detected on the surface of the test specimen is found to have a marked effect of upsetting the temperatures computed for

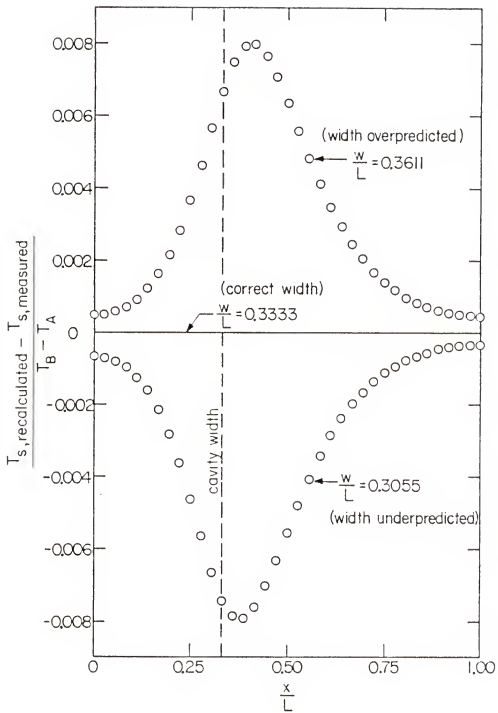

Figure 6

Recheck of Cavity Wall Position in Problem 1

interior nodes. The region affected spreads out covering an angle

$$\theta = 2 \tan^{-1}\frac{(\Delta x)}{(\Delta y)}$$

with the point of irregularity positioned at the apex. Fortunately, such an irregular temperature can often be detected in practice and can therefore be corrected before analysis.

A point of interest is that, because of the plane wall system addressed in this study, two limiting cases occur. The surface temperature observed at the edge of the system (i.e., point E in Fig. 5) is expected to asymptotically reach that of a plane wall of thickness ℓ, if the cavity width is small; i.e.,

$$\frac{T_S - T_A}{T_B - T_A} = 1 - \frac{1}{1 + \frac{k}{h\ell}} \tag{10}$$

By the same token, the surface temperature observed at the center of the cavity will reach asymptotically that of a plane wall of thickness (ℓ-d), if the cavity is large. These limiting cases permit one to find a better k/h value and use it in the analysis. This point can be illustrated by referring to the surface temperature data given in Fig. 5. Using the surface temperature at point E and equation (10), one finds hL/k = 9.9238, an error of 0.76% (note the correct value is 10). If the surface temperature at point F is used, the predicted $\frac{hL}{k}$ is 10.0793, again a small error of 0.79%. It is noted that the cavity shown in Fig. 5 is a middle size one. A wider cavity will make the prediction based on the surface temperature at the cavity center even more accurate, and vice versa. One should be cautioned, however, that in the present study the convective coefficient has been assumed to be a constant. In the event that a deep capity is encountered, the surface temperature differential between center and edge of the

system may become appreciable. Under these conditions, the variation of h with T should also be considered and an accurate prediction becomes more difficult.

The methodology presented above was developed into a computer program for a computer-based prediction operation. A block diagram showing the computer logic is given in Fig. 7.

Extension to Two Dimensional Systems

The analysis presented above can be applied to predict cavity geometry in a two-dimensional system such as a rectangular cross-sectioned hole in a parallelepiped. If the length of this body is very long along the hole axis such that the temperature variation along this axis is negligible, the interior nodal temperatures can be computed in a two-dimensional array. There are four surfaces now available for measuring temperatures; each of these surface temperatures can be used to compute interior nodal temperatures with one set calculated for each direction of computation. In this way the position of the nearest hole boundary that is parallel to the surface can be determined. By superimposing these four arrays of temperatures, the hole configurations can be identified. In fact, chores of recalculating and matching surface temperatures in this two dimensional system can be totally eliminated in the process. It should be noted that, while the method of prediction of cavity geometry becomes easier for this two dimensional system, the accuracy of prediction becomes heavily dependent on the h/k value used in the analysis. Of major concern to users is the fact that, for two dimension systems, there are no limiting cases (as one had before) to check this h/k value.

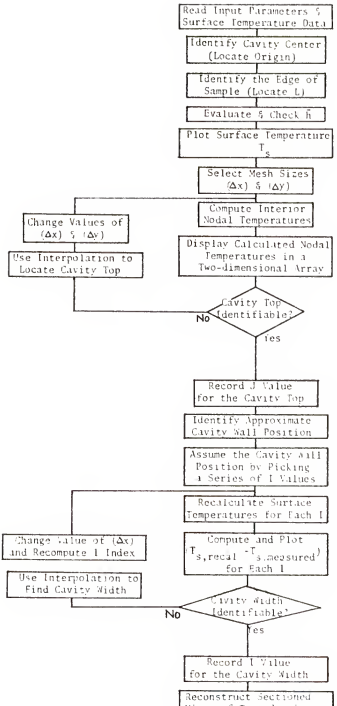
Read Input Parameters & Surface Temperature Data
Identify Cavity Center (Locate Origin)
Identify the Edge of Sample (Locate L)
Evaluate & Check h
Plot Surface Temperature T_s
Select Mesh Sizes (Δx) & (Δy)
Change Values of (Δx) & (Δy)
Compute Interior Nodal Temperatures
Use Interpolation to Locate Cavity Top
Display Calculated Nodal Temperatures in a Two-dimensional Array
Cavity Top Identifiable?
No
Yes
Record J Value for the Cavity Top
Identify Approximate Cavity Wall Position
Assume the Cavity Wall Position by Picking a Series of I Values
Recalculate Surface Temperatures for Each I
Change Value of (Δx) and Recompute I Index
Compute and Plot ($T_{s,recal}$ - $T_{s,measured}$) for Each I
Use Interpolation to Find Cavity Width
Cavity Width Identifiable?
No
Yes
Record I Value for the Cavity Width
Reconstruct Sectioned Views of Test Specimen

Figure 7

Flow Diagram Showing Procedures to Evaluate Cavity Geometry in Problem 1

A sample case is shown in Fig. 8 where the test conditions are specified in the legend. The surface temperature data were again calculated using an iteration scheme* and plotted in the figure in open circles surrounding the test body. These surface temperatures were subsequently used as inputs to predict the hole geometry.+ For example, the isotherm at $(T-T_A)/(T_B-T_A)=1$ predicted based on the bottom surface temperature is plotted using solid lines inside the center figure; the computation approaches from below. By superimposing four isotherms the geometry of the hole can be identified. The predicted hole agrees well with the actual hole (see tick marks on the body boundaries) except the corners are slightly rounded, a result of the data smoothing as has been discussed previously. Clearly, the method presented here is convenient to use and is more accurate than any other methods reported in the literature.

*A computer program useful for this part of the work is presented in Appendix D.

+A computer program used to solve this inverse problem is included in Appendix E.

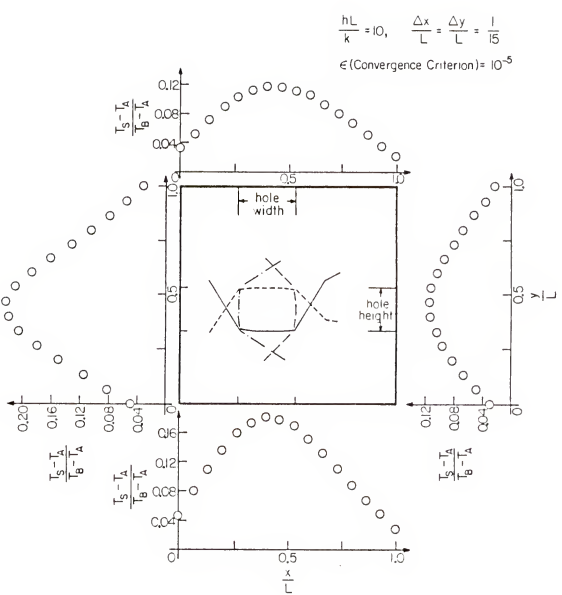

Figure 8

Prediction of Hole Geometry in a Parallelepiped in Problem 1

CHAPTER III

PROBLEM 2: BOUNDARY CONDITION OF THE SECOND KIND AT THE CAVITY SIDE

For a constant heat flux applied on the lower boundary, the methodology presented in Problem 1 cannot be used to predict the cavity top. The problem lies in the fact that the temperature at the cavity boundary is now an unknown. On the other hand, the heat flux is not suitable as an identifier for cavity boundary either because, away from the cavity (side) wall, the heat flux is constant at every point in the heat flow direction. It is significant to note that the surface temperature pattern observed is also different for this problem. Unlike Problem 1, which has a hot spot above the cavity center, the hot spot for Problem 2 moves to the vicinity of the cavity (side) wall. This point will be examined later.

The determination of the cavity depth in Problem 2 can be made by using the measured top surface temperature. In this instance, the total heat Q_t dissipated from the surface can be integrated using Newton's Law. For a constant heat flux f applied on the lower boundary, the depth of the cavity can be determined using a simple relation

$$d = \frac{Q_t}{f} - L \tag{11}$$

which is derived based on the simple analysis that energy is conserved. This notion greatly simplifies the problem as the width of the cavity now becomes the only unknown for investigation. It is found that an analytical approach is convenient to find this width. The derivation of equations follows below.

Analysis

The system under investigation can be formulated in terms of dimensionless groups as,

$$\nabla^2 U = 0 \tag{12}$$

where

$$U = U(\xi,\eta)$$

subjected to boundary conditions,

$$\frac{\partial U(\omega,\eta)}{\partial \xi} = -\frac{fL}{kT_A} \qquad 0 \leq \eta \leq \delta \tag{12a}$$

$$\frac{\partial U(0,\eta)}{\partial \xi} = 0 \qquad \delta \leq \eta \leq \mu \tag{12b}$$

$$\frac{\partial U(1,\eta)}{\partial \xi} = 0 \qquad 0 \leq \eta \leq \mu \tag{12c}$$

$$\frac{\partial U(\xi,\delta)}{\partial \eta} = -\frac{fL}{kT_A} \qquad 0 < \xi \leq \omega \tag{12d}$$

$$\frac{\partial U(\xi,0)}{\partial \eta} = -\frac{fL}{kT_A} \qquad \omega \leq \xi < 1 \tag{12e}$$

$$\frac{\partial U(\xi,\mu)}{\partial \eta} = -Bi\ U(\xi,\mu) \qquad 0 < \xi < 1 \tag{12f}$$

In the above equations the dimensionless groups are defined as,

$$U = \frac{T(x,y) - T_A}{T_A},\ \xi = \frac{x}{L},\ \eta = \frac{y}{L},\ \omega = \frac{w}{L},\ \delta = \frac{d}{L},\ \mu = \frac{\ell}{L},\ Bi = \frac{hL}{k}$$

A diagram of the system is shown in Fig. 9.

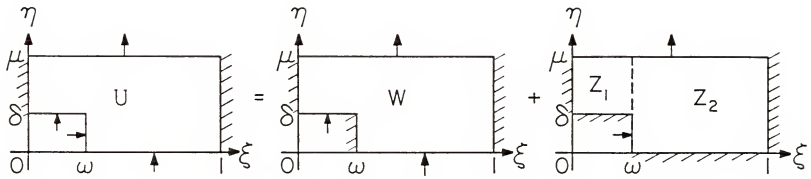

Figure 9

Illustration of a Superposition Technique

The problem U can be divided into two subproblems using the superposition technique,

$$U(\xi,\eta) = W(\xi,\eta) + Z(\xi,\eta) \tag{13}$$

The subproblem W satisfies the governing equation,

$$\nabla^2 W = 0 \tag{14}$$

and the boundary conditions:

$$\frac{\partial W(\omega,\eta)}{\partial \xi} = 0 \qquad 0 \leq \eta \leq \delta \tag{14a}$$

$$\frac{\partial W(0,\eta)}{\partial \xi} = 0 \qquad \delta \leq \eta \leq \mu \tag{14b}$$

$$\frac{\partial W(1,\eta)}{\partial \xi} = 0 \qquad 0 \leq \eta \leq \mu \tag{14c}$$

$$\frac{\partial W(\xi,\delta)}{\partial \eta} = -\frac{fL}{kT_A} \qquad 0 < \xi \leq \omega \tag{14d}$$

$$\frac{\partial W(\xi,0)}{\partial \eta} = -\frac{fL}{kT_A} \qquad \omega \leq \xi < 1 \tag{14e}$$

$$\frac{\partial W(\xi,\mu)}{\partial \eta} = -\mathrm{Bi}\, W(\xi,\mu) \qquad 0 < \xi < 1 \tag{14f}$$

A pictorial presentation of these conditions is given in the middle diagram of Fig. 9.

The subproblem Z satisfies the governing equation,

$$\nabla^2 Z = 0 \tag{15}$$

and the boundary conditions:

$$\frac{\partial Z(\omega,\eta)}{\partial \xi} = -\frac{fL}{kT_A} \qquad 0 \le \eta \le \delta \tag{15a}$$

$$\frac{\partial Z(0,\eta)}{\partial \xi} = 0 \qquad \delta \le \eta \le \mu \tag{15b}$$

$$\frac{\partial Z(1,\eta)}{\partial \xi} = 0 \qquad 0 \le \eta \le \mu \tag{15c}$$

$$\frac{\partial Z(\xi,\delta)}{\partial \eta} = 0 \qquad 0 < \xi \le \omega \tag{15d}$$

$$\frac{\partial Z(\xi,0)}{\partial \eta} = 0 \qquad \omega \le \xi < 1 \tag{15e}$$

$$\frac{\partial Z(\xi,\mu)}{\partial \eta} = -\,\mathrm{Bi}\; Z(\xi,\mu) \qquad 0 < \xi < 1 \tag{15f}$$

Figure 9 again depicts these conditions pictorially.

In the solution of problem W, the insulated cavity walls enable one to drop the ξ dependency in the analysis. The top surface temperature is uniform and can be derived by equating equations (14d), (14e), and (14f), giving,

$$W(\mu) = \frac{f}{hT_A} \tag{16}$$

Because of the irregular shape of the system, problem Z cannot be solved by classical means. However, the entire region of the system can be subdivided into two parts, Z_1 and Z_2 as shown in Fig. 9. Be mindful that the purpose of the present study is to determine the cavity geometry based on an additional measured temperature on the top surface. Then, if the problem Z_1 is solved first, the measured surface temperature can be used to determine the heat flux across the dashed boundary between regions Z_1 and Z_2. Based on this crosswise heat flux, the temperature on the top surface of Z_2 can also be predicted. A correct cavity width is one where this predicted temperature matches the measured value . A trial and error is still needed

to find the exact wall position. However, since the location of the peak surface temperature should be near the cavity wall, the trials will not be made blindly.

Attention is now directed to the solution of the Z problem; problem Z_1 is treated first. Let the cross heat flux be denoted as g, $Z_1(\xi,\eta)$ can be derived using the separation of variables technique as:

$$Z_1(\xi,\eta) = \sum_{n=1}^{\infty} \frac{1}{\lambda_n \sinh\lambda_n \omega} \frac{2(\lambda_n^2 + Bi^2)}{(\mu-\delta)(\lambda_n^2 + Bi^2)+Bi} \cosh\lambda_n \xi \cos\lambda_n (\eta-\delta) \int_0^{\mu-\delta} g(\nu)\cos\lambda_n \nu d\nu \tag{17}$$

which is valid for $0 \leq \xi \leq \omega$, $\delta \leq \eta \leq \mu$. λ_n are the roots of $\lambda_n \tan\lambda_n (\mu-\delta) = Bi$.

The temperature at the top surface can be found by substituting μ for η in the above equation and rewriting it as follows:

$$Z_1(\xi,\mu) = \sum_{n=1}^{\infty} \frac{\cos\lambda_n(\mu-\delta)}{\lambda_n \sinh\lambda_n \omega} \frac{2(\lambda_n^2+Bi^2)}{(\mu-\delta)(\lambda_n^2 + Bi^2) + Bi} \cosh\lambda_n \xi \int_0^{\mu-\delta} g(\nu)\cos\lambda_n \nu d\nu \tag{18}$$

where $0 \leq \xi \leq \omega$. Since this surface temperature is known, there in only one unknown $g(\nu)$ in the above equation. To solve for this $g(\nu)$ one has to replace the integral by a summation using Simpson's rule as:

$$\int_0^{\mu-\delta} g(\nu)\cos\lambda_n \nu d\nu = \frac{\Delta\nu}{3} [G_1 + 4(G_2 + G_4 \ldots + G_{m-1}) + 2(G_3 + G_5 + \ldots + G_{m-2}) + G_m] \tag{19}$$

where,

$$G_i = g[(i-1)(\Delta\nu)]\cos\lambda_n(i-1)(\Delta\nu) \tag{20}$$

and i=1, 2, ...m

With this substitution, the terms in equation (18) can be regrouped as follows.

$$Z_1(\xi,\mu) = g(0)\sum_{n=1}^{\infty} C_n\cosh\lambda_n\xi + 4g(\Delta\nu)\sum_{n=1}^{\infty} C_n\cosh\lambda_n\xi\cos\lambda_n(\Delta\nu)$$

$$+ 2g(2\Delta\nu)\sum_{n=1}^{\infty} C_n\cosh\lambda_n\xi\cos\lambda_n 2(\Delta\nu) + \ldots$$

$$+ g[(m-1)(\Delta\nu)]\sum_{n=1}^{\infty}\cosh\lambda_n\xi\cos\lambda_n(m-1)(\Delta\nu) \tag{21}$$

where,

$$C_n = \frac{(\Delta\nu)\cos\lambda_n(\mu-\delta)}{3\lambda_n\sinh\lambda_n\omega} \quad \frac{2(\lambda_n^2+Bi^2)}{(\mu-\delta)(\lambda_n^2+Bi^2)+Bi} \tag{22}$$

$g(\nu)$ can then be solved using the method of simultaneous linear equations. It is noted that, to make the matrix multiplication compatible in the solution, the number of unknowns in g must be chosen to be equal to the number of Z_1 used as inputs.

The solution of problem Z_2 can again be made using the separation of variables technique. The top surface temperature distribution is,

$$Z_2(\xi,\mu) = \sum_{m=1}^{\infty} \frac{1}{\lambda_m\sinh\lambda_m(1-\omega)} \quad \frac{2(\lambda_m^2+Bi^2)}{(\lambda_m^2+Bi^2)+Bi}\cosh\lambda_m(1-\xi)\cos\lambda_m\mu$$

$$\left(\frac{fL}{kT_A}\frac{1}{\lambda_m}\sin\lambda_m\delta - \int_0^{\mu} g(\eta)\cos\lambda_m\eta d\eta\right) \tag{23}$$

which is valid in the range of $\omega \leq \xi \leq 1$. The eigenvalues λ_m are roots of

$$\lambda_m \tan\lambda_m \mu = Bi$$

The crosswise heat flux determined earlier can be used to solve the integral in equation (23).

It is noted that the boundary condition chosen in the analysis at the interface between Z_1 and Z_2 is a nonhomogeneous condition of the second kind. This condition is of the same kind as that imposed on the cavity (side) wall; hence, a mixed boundary problem will not result in the analysis.

Clearly, the method presented above is an exact solution. One may wonder why the present problem is not treated numerically as was done before in Problem 1. The problem lies in the fact that, for Problem 2, because of the boundary conditions, none of the boundary temperatures are known. In fact, the problem becomes an ill-conditioned one to the extent that it cannot be solved numerically using an iteration scheme [24]. Of course, the Gaussian elimination and the matrix inversion methods are still useful. They may pose a problem to computer storage, if the system under investigation is excessively large.

Conversely, a similar analysis could have been made to solve Problem 1 using the exact solution presented in this section. But the boundary conditions for Problem 1 are so tedious that, even with a nonhomogeneous boundary condition of the first kind imposed on the interface (between Z_1 and Z_2) and with a changing of the reference temperature level, there are still two nonhomogeneous boundary conditions appearing in each of the subproblems of Z. This requires a further superposition in the solution, which makes the exact solution too complicated to use in the previous problem.

Example and Discussion

Tests were made to validate the methodology presented in this section. Gaussian elimination was used to compute the temperature in plane walls with specified cavity geometries and heat fluxes.* The surface temperatures obtained from these models were subsequently used as inputs to an inverse problem to predict the cavity geometry. A sample case is presented in Fig. 10 where test conditions are given in the legend.

As has been previously discussed, the hot spot on the surface is now located near the cavity wall. The peak point on the temperature curve is also displaced away from the cavity center. This phenomenon can again be ascribed to the additional heat flux that penetrates the cavity (side) wall.

An attempt was next made to predict the cavity width based on the precalculated cavity depth using equation (11), see Fig. 11. Using the surface temperature data right above the actual cavity region to recalculate surface temperatures at points beyond the cavity width, yields data that match with the measured surface temperatures within -0.08 to 0.11%. This is identified by a band of data spread, as shown on the right side scale of the figure.+ It is also noted that this good result was found using only five terms in the Simpson's rule, equation (19). An underprediction of cavity width by one mesh size (Δx) yields recalculated surface temperatures in the range of $\frac{4}{12} \leq \frac{x}{L} \leq 1$ different from the measured values; see open circles. The trend of data is totally reversed if the cavity width

*A generalized computer program capable of solving this direct problem is given in Appendix F.

+Computer program for this example is included in Appendix G.

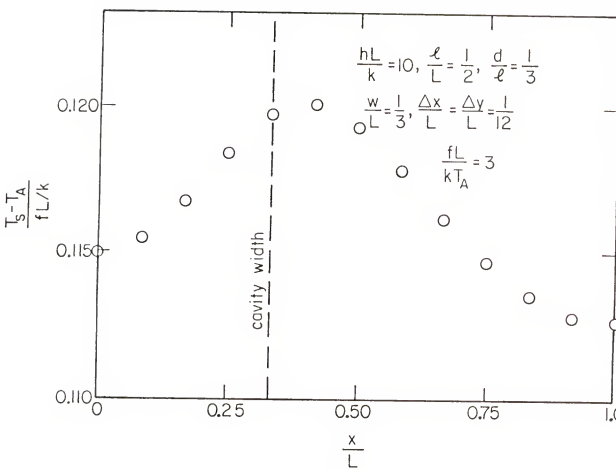

Figure 10

Use of Surface Temperatures to Predict Cavity Geometry
in Problem 2

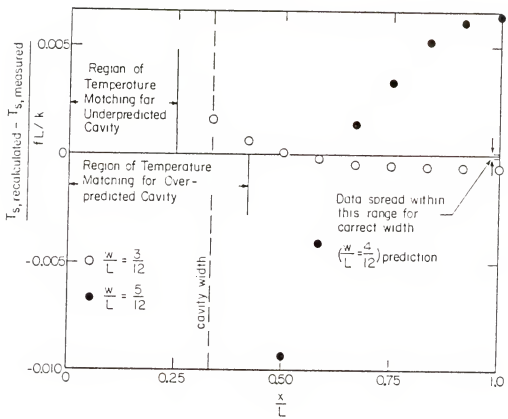

Figure 11

Recheck of Cavity Wall Position in Problem 2

is overpredicted by one mesh size; see closed circles in the figure. Because the method of checking the cavity width in Problem 2 is different from that used in Problem 1, it is expected that the present data will not bear resemblance to that of Fig. 6. However, by examining the surface temperatures in the matched region (Z_1), one can still find a trend in the data observed. This can be seen by referring to the surface temperature shown in Fig. 10. Near the cavity wall, between points $\frac{x}{L} = 0.25$ and 0.33, the dimensionless temperature slope is 0.05225. This is fairly close to that found between points $\frac{x}{L} = 0.1667$ and 0.25; its value is 0.0635. However, the slope between points $\frac{x}{L} = 0.33$ and 0.4167 is 0.00106, which is 80% lower than needed (0.05225). As a result the temperatures, recalculated right to the predicted (cavity) width on Z_2 for the overpredicted case, will change drastically from what one would obtain for a perfectly matched case. Discussion on the prediction of cavity width is now complete; attention will now be directed to the error analysis, as follows.

The error analysis for Problem 2 is much easier to handle than that of Problem 1. Use of an overestimated h will increase Q_t (see equation (11)) thereby leading to an overprediction of cavity depth. This trend is reversed if a smaller h is used in the analysis. However, an estimation of h using surface temperatures at the center and the edge of the system does not meet with equal success. According to Newton's Law,

$$T_S - T_A = \frac{f}{h} \tag{24}$$

which is strictly valid at points remote from the cavity (side) wall. Using this equation and the surface temperature given in Fig. 10, one

computes $(f/hT_A) = 0.3381$, which is based on the surface temperature at the edge of the system; note the correct value is 0.3, hence, a 12.7% overprediction. A prediction of this parameter based on the surface temperature at the center of the system yields $(f/hT_A) = 0.3453$, a 15.1% overprediction. Again, a better prediction can probably be made based on the edge temperature, if the cavity is very narrow and vice versa.

The methodology presented above is again developed into a computer program for a computer-based prediction operation. A block diagram showing computer logic is given in Fig. 12.

Extension to Two Dimensional Systems

The analysis presented above can be extended to predict cavity geometry in a two-dimensional system* such as the one shown in Fig. 13. A simple analysis equating heat injected to the walls of the hole with the heat dissipated from the surfaces of the body, provides input to predict the hole geometry. The method goes as follows.

For the rectangular hole in the parallelepiped, heat can be freely dissipated from four exposed surfaces. As a result, the surface temperature distribution will not be the same as what one would observe on a plane wall (Fig. 10); there is a temperature peak appearing on each of the exposed surfaces. Then, if one erects sectioned planes perpendicular to the surface and passes through these peak points, these erected planes can be regarded as adiabatic planes for heat flow; see dash-dotted lines in Fig. 13. Using these sectioned planes, the entire system can be divided into four quadrants which are labeled in Roman Numerals in the figure. The problem boils down to the determination of the values of a

*A generalized computer program capable of solving this direct problem is given in Appendix H.

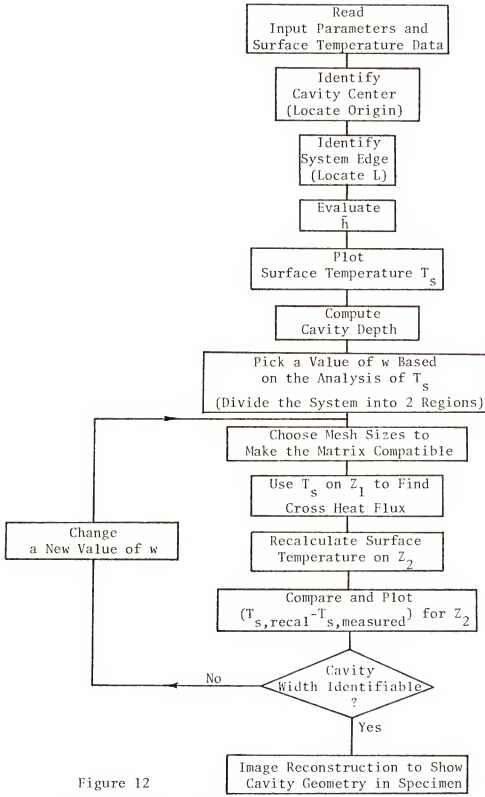

Figure 12

Flow Diagram Showing Procedures to
Evaluate Cavity Geometry in Problem 2

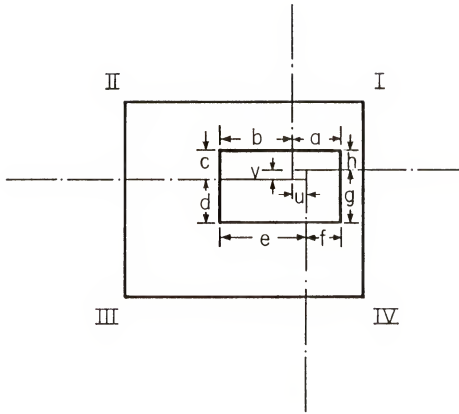

Figure 13

Partition of Hole into Four Quadrants in a Two-dimensional Analysis

through h eight variables in the figure. This can be done by writing the following six relations:

$$a + b = e + f \tag{25}$$

$$c + d = g + h \tag{26}$$

$$a + h = \frac{Q_I}{f} \tag{27}$$

$$b + c = \frac{Q_{II}}{f} \tag{28}$$

$$d + e = \frac{Q_{III}}{f} \tag{29}$$

$$f + g = \frac{Q_{IV}}{f} \tag{30}$$

where equations (25) and (26) are suggested by geometry; equations (27) to (30) are based on the heat transfer analysis. The total heat dissipation Q in the above equations can be calculated based on the measured surface temperatures and the convective coefficient h. In addition, two equations can be written based on the relative locations of the temperature peak points. Comparing the location of these points on two opposite surfaces yields:

$$|a-f| = u \tag{31}$$

$$|g-d| = v \tag{32}$$

where u and v can be found experimentally.

It is important to note that, while equations (25) to (32) appear to form a set of eight simultaneous linear equations, one of the equations among (27) to (30) is actually not independent, which can be proved by considering a special case when u = v = 0. To generate an additional condition would require an elaborate analysis of evaluating and rematching surface temperatures as has been discussed previously in the one-dimensional

analysis. However, if two adjoining surfaces of the hole are located equidistant from the surface (of the system), which can be detected by the symmetry of surface temperatures near the corner, an additional adiabatic plane can be located at this corner. Thus for this simplified case, one of the hole dimensions can be readily determined.

A sample case is shown in Fig. 14. This time the surface temperatures, calculated using Gaussian elimination for the given hole geometry, are plotted in figures surrounding the body, where the test conditions are also delineated in the legend (upper right corner). These surface temperatures are successively used as inputs in equations (25) to (32) to predict the hole geometry. For the system shown, the adiabatic planes (dash-dotted lines) are determined from the peak temperatures on the curves; u and v appear to be zero. Also, since the surface temperatures observed on the left lower corner of the body (see center figure) are symmetric, an additional adiabatic plane can be identified and located at this corner. This permits the dimension e(=b) to be determined based on the heat dissipation from the surface, the calculated value there is 0.2275, which is 1.1% overpredicted (true value = 0.225, see center figure). Using this value of e(=b), values of a(=f), c(=h), and d(=g) can be calculated to be 0.1941, 0.3058 and 0.2725, respectively. These values are accurate to within 1.3% of the true hole geometry; the errors are primarily numerical.

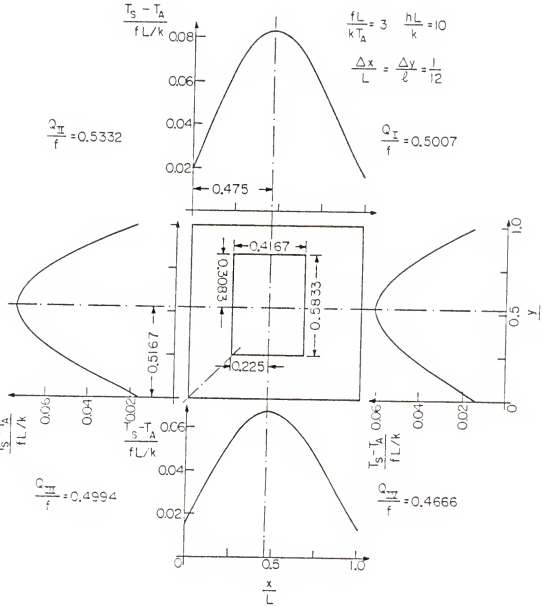

Figure 14

Prediction of Hole Geometry in a Parallelepiped in Problem 2

CHAPTER IV

PROBLEM 3: BOUNDARY CONDITION OF THE THIRD KIND AT THE CAVITY SIDE

For a convective condition appearing on the cavity side, neither the temperature nor the heat flux is available at this boundary. Without these clues, the problem would be impossible to solve using the methods given in the preceding two chapters. To avoid a grand-scale trial-and-error solution, a pattern recognition scheme is attempted as shown in this chapter.

Pattern Recognition Theory

In the pattern recognition theory, there are three approaches one can use to recognize patterns; they are the membership-roster approach, the common-property approach and the clustering approach. The membership-roster approach requires that sets of patterns belonging to various pattern classes be stored in the pattern recognition system. Then, if an unknown pattern is shown in the system, this pattern is compared to the stored patterns one by one. The pattern recognition system is constructed such that the input pattern is classified as a member of a pattern class, if this pattern matches one of the stored patterns belonging to that class. This approach is simple and will work if the pattern samples are ideal (i.e., noise-free). There is also a drawback in this approach in that a pattern recognition system designed on the basis of this membership-roster approach demands a large memory for storing patterns.

The common-property approach is able to resolve the storage problem in the membership-roster approach. The basic assumption in the common-property approach is that patterns belonging to the same class should possess certain common properties or attributes that reflect the similarity among these patterns. Based on this assumption, there is no need to store the entire pattern in the memory as in the membership-roster approach; only pattern properties or attributes need be stored. Then, when an unknown pattern is shown to the system, its features are extracted from the pattern and these features are matched with those stored features to make classifications.

Clearly, the success of the common-property approach relies heavily on the selection of features. If the features of a pattern are selected properly that truly characterize the class of patterns they belong to and if the features are precisely determined from a large group of sample patterns, the common-property approach can be made a very powerful tool to identify patterns.

The clustering approach is useful when patterns can be expressed as pattern vectors in the pattern space. If the points representing patterns in the same class are congregated to form clusters in this space and, if these clusters are spaced far apart, simple recognition schemes such as the minimum-distance classification technique can be used to classify patterns.

It is noted that, in the present application of nondestructive testing using surface temperature profiles, the pattern recognition theory will be used in a slightly different way. The problem lies in the fact that one is not interested in differentiating a good sample

(without cavity) from a bad sample (with cavity), but in predicting how extensive the cavity is behind the surface. And, this is done based on the analysis of a large number of patterns, all taken from the bad samples. In this context, since there is an infinite number of ways of combining the cavity widths and depths, using the membership-roster approach would require storage of an infitite number of patterns in the memory. By the same token, the pattern space would also be fitted with pattern points to the extent that no clustering of points can ever be found in this space.

Nevertheless, the common-property approach is still useful. For a rectangular cavity appearing behind the surface, the observed surface temperature has a peak point, a minimum point and an inflection point in the profile. These features can be found from all temperature profiles and can be correlated as functions of cavity width and depth. Then, once these functions are found, the pattern recognition is ready. In the section that follows, this common-property approach will be employed to make pattern recognition and used to predict cavities. The sample patterns to be used in the correlation will be generated first using numerical solutions.*

Example and Discussion

For the system shown in Fig. 1, the surface temperature is evaluated using a finite difference method. Since the problem is ill-conditioned, Gaussian elimination must be used to solve simultaneous equations. Data used as input in the solution are summarized in Table 1. For the problem at hand, Reynold's number at the lower boundary is arbitrarily

*A computer program used to evaluate surface temperatures is given in Appendix I.

TABLE 1

Input Data for a Numerical Solution of Surface Temperatures for a Problem Having a Boundary Condition of the Third Kind at the Cavity Side

Specimen Sizes:

$L = 1.0$ ft

$\ell/L = 0.25$

Mesh Sizes:

$\Delta x/L = 0.04167$

$\Delta y/L = 0.04167$

Cavity Sizes:

$d/L = 0.1667 \sim 0.6667$ (4 cases)

$w/L = 0.1667 \sim 0.6667$ (6 cases)

Thermophysical Property:

$k = 0.01731$ W/cm°C (=1.0 Btu/hrft°F)

Ambient Temperatures:

$T_a = 93.3$°C (=200°F)

$T_A = 25$°C (=77°F)

Top Surface - Free Convection*[25]:

$$h_A = 0.27 \left(\frac{T_S - T_A}{L}\right)^{1/4}$$

Lower Surface - Forced Convection+[26]:

$$Nu = \frac{h_a L}{k} = 0.205 \, (Re)^{0.731}$$

*Variables in this empirical equation are in British Units.

+Empirical constants given in the equation are for Re = 4,000 ~ 15,000

chosen to be 8,000. On the top surface, the free convective coefficient h_A is treated as a variable; the coefficient is a function of the unknown surface temperature T_s. Hence, an iteration procedure is used in the solution to repeatedly calculate the surface temperatures until it converges to a prescribed limit (ε=0.0056°C or 0.001°F). A sample output of the surface temperature is shown in Fig. 15.

The numerical method was used to generate sample patterns for twenty-four combinations of cavity widths and depths. Feature data were extracted from these patterns and correlated as shown in Figs. 16-18. Some observations can be made based on these figures.

In Fig. 16 the point of inflection x is shifted away from the cavity center as the cavity widens, which is not unexpected. The point of inflection appears to be weakly dependent on the cavity depth; see data bands and the sets of cavity depth data plotted for each width on the right of the figure. This trend suggests that the point of inflection alone can be used to predict the cavity width if a small error is tolerable. An equation correlated based on a least square linear fit is given as follows:

$$\frac{x}{L} = 0.051 + 0.992\ \frac{w}{L} \tag{33}$$

which is plotted as a continuous line in the figure. The dashed lines represent an error range arising from the depth dependency. The error is largest ($\pm$3%) at w/L=0.5 and drops off slightly toward larger and smaller widths.

The peak surface temperature also increases monotonically with the cavity depth; see Fig. 17. Here, the width dependence is shown using bands and a figure showing the dependence of the peak temperatures on

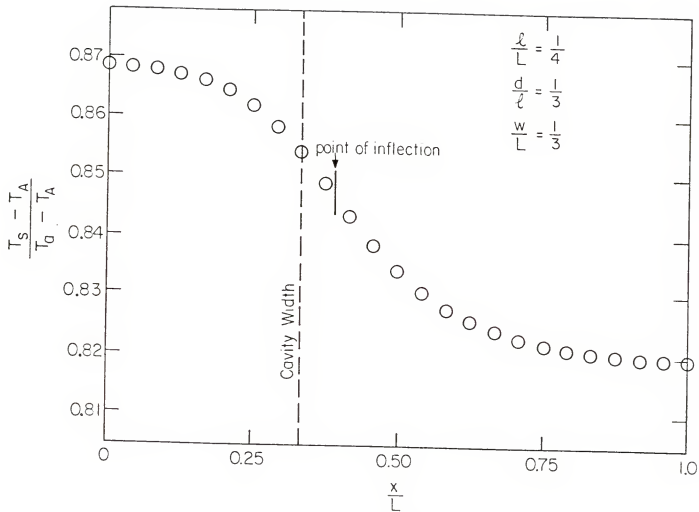

Figure 15

Sample Output of a Surface Temperature Pattern in Problem 3

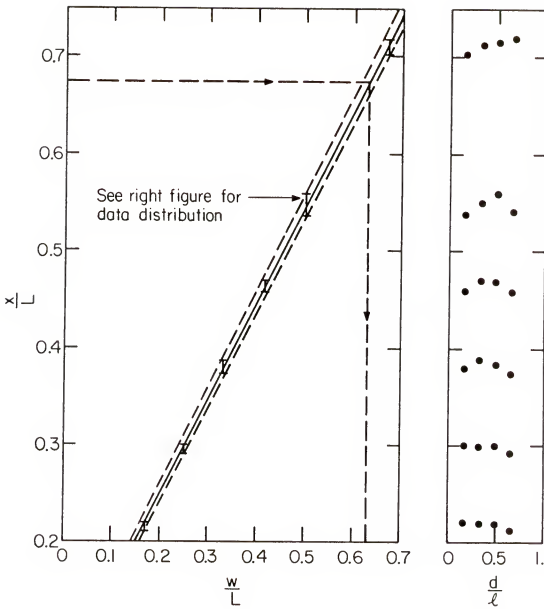

Figure 16

A Plot of Inflection Point Location Versus
Cavity Width and Depth in Problem 3

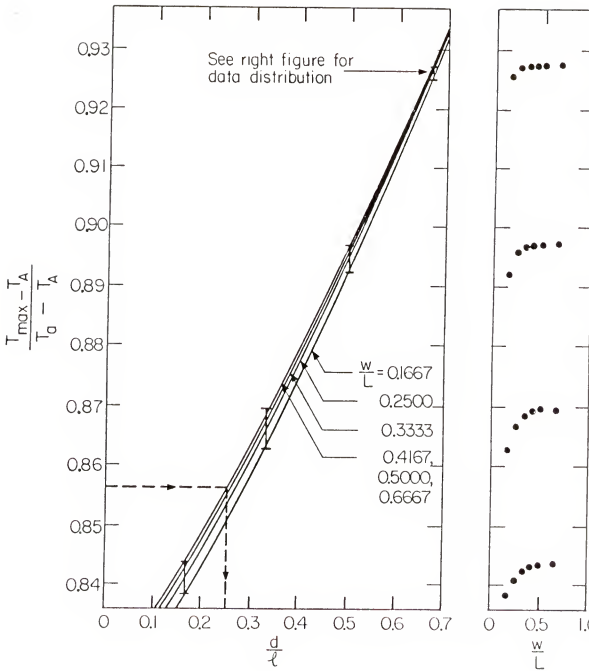

Figure 17

A Plot of Peak Surface Temperature Versus Cavity Depth and Width in Problem 3

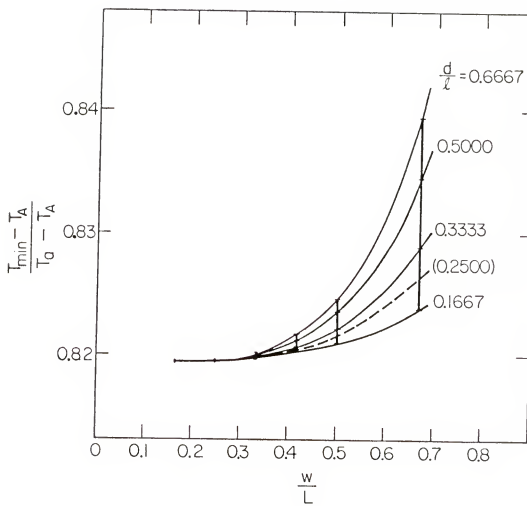

Figure 18

A Plot of Edge Surface Temperature Versus
Cavity Depth in Problem 3

widths as various depths is provided on the right of the figure. These bands appear to be narrower toward larger depths; also, when the cavity is deepened the width dependence tends to level off at smaller widths. The peak temperature can be related to the cavity width and depth using a least-squares parabolic fit. It is formulated as follows:

$$T_{max} = A + B\left(\frac{d}{\ell}\right) + C\left(\frac{d}{\ell}\right)^2 \tag{34}$$

where,

$$A = 177.89 - 0.33\ \left(\frac{w}{L}\right) \tag{35}$$

$$B = -0.06 + 76.71\ \left(\frac{w}{L}\right) - 78.34\ \left(\frac{w}{L}\right)^2 \tag{36}$$

$$C = 27.76 - 103.2\ \left(\frac{w}{L}\right) + 103.6\ \left(\frac{w}{L}\right)^2 \tag{37}$$

The minimum temperature correlation is shown in Fig. 18. In this figure, the minimum temperature does not have sufficient resolution to identify small cavities. In practice, this minimum temperature is measured far away from the cavity wall and should reach, asymptotically, that of a plane wall without cavities. Hence, this minimum temperature should be invariant with samples and, as such, has to be disqualified as a feature.

The error in the prediction is limited primarily to that by the correlation. A development of an error chart met with no success. As a means of checking our correlations, a test is run using the computer to generate the surface temperature data for a test case of w/L=0.625 and d/ℓ=0.25. The maximum temperature and the inflection point found from the computed surface temperature are 83.52°C (182.33°F) and 0.675, respectively. By using these values in the correlated equations (33) and (34), the predicted cavity width and depths are 0.629 and 0.2545, respectively, an overprediction of 0.6% (width) and 1.8% (depth).

An alternative approach is to use charts instead of correlation equations. Following the arrows in Fig. 16, the cavity width can be found, using the continuous line, to be 0.63. Next, Fig. 17 is used. This time, since a family of curves is available, one picks the curve of $w/L=0.6667$ and find $d/\ell=0.25$. This d/ℓ enables the w/L prediction to be refined by returning to Fig. 16. In this instance, since $d/\ell=0.25$ is already located near the center of the depth band, no further correction of the width appears possible. In fact, this first loop of prediction yields values which are surprisingly accurate.

It is noted that, while using the chart is more accurate, the use of correlation equations is convenient for a computer operation. A flow diagram giving such an operation is shown in Fig. 19.

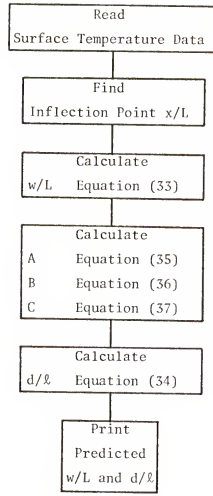

Figure 19

Flow Diagram Showing Procedures to Evaluate Cavity Geometry Using Correlation Equations

CHAPTER V

CONCLUSIONS

The scanned surface temperature data from a body is used to predict the cavity lying underneath the surface. The basic system under investigation is a plane wall having a rectangular cavity at the back surface. The front surface dissipates heat by convection; this is also the surface whose surface is scanned. Three types of boundary conditions are considered on the back surface. For a prescribed surface temperature specified on the cavity side, a numerical solution is found convenient to predict the cavity top and the approximate location of the cavity wall. A recheck of the cavity wall position calls for matching the recalculated surface temperature with the measured temperature. The data are found to be well behaved to the extent that an interpolation is possible when the mesh size chosen happens to miss the wall position.

In the second problem, the heat flux at the cavity side is given. Using this heat flux, the cavity depth can be determined. An exact solution is found convenient for this case to check the cavity wall position. The method used is to divide the system about the cavity into two regions and use the additional surface temperature observed above the cavity top to find a cross heat flux between the divided regions. In this way the surface temperature on the remaining boundary can be recalculated and used to match the measured temperature.

For a convective condition appearing on the cavity side, neither of the aforementioned methods works. A pattern recognition method using the common-property approach must be used.

The methodologies developed for the first two types of problems (prescribed temperature or heat flux at the cavity side) are also extended to predict holes in parallelepipeds. In contrast to what one might expect, because of additional surface temperatures available for analysis, the prediction method turns out to be less sophisticated. Accuracy is also good if the cavity side has a prescribed temperature. The method is slightly restrictive if a heat flux is specified at the cavity side. In this latter instance, a symmetric corner must be located and the method only works for this special case.

An approximate solution relating the surface temperature with the cavity geometry is also developed in this work. A superposition technique is used for solution, and the solution gives a good estimation of the surface temperatures for systems having rectangular cavities. Since the solution is only approximate, its use to predict cavity is not recommended.

CHAPTER VI

RECOMMENDATIONS

The methodology developed in this work is valid for a steady state system with heat injected into the back (cavity) side of the specimen and with the front (convective) surface scanned to measure its temperature. There are several other modes by which the specimen can be tested. For example, the specimen can be preheated to a uniform temperature and then the front surface suddenly cooled by using an impulsive ambient temperature change. The front surface temperature-time history is scanned and used to predict the cavity. This way of operation has been proposed by [18] to determine the temperature-dependent volume heat source term in the governing equation and can also be used here for cavity prediction.

Another method of operation, quite similar to the above, allows heat to travel in the opposite direction. The method is to inject heat through the front surface and also use this front surface for scanning and monitoring temperature changes. As heat penetrates into the specimen any irregularity behind the surface should affect the temperature distribution and be manifested on the surface.

Both of these new methods appear to be easier to use than the ones presented in this study, but their accuracy may be poorer unless one can precisely adjust the boundary condition at the cavity side as one desires.

Another system of great engineering importance is a cavity located within the medium. For this new system the aforementioned methods appear to be highly favorable. Again, methodologies are lacking for testing this new condition.

The methodologies developed based on analytical studies are usually handicapped because of the need to assume a constant convective coefficient in the analysis. In practice, the surface temperature is not uniform; hence the convective coefficient must be treated as a variable in the analysis. Because of this disparity, it is imperative to use experiments to validate the proposed methodologies. Also the experiment permits a revelation of the true limitations of the method an analytical study is not able to do. The experiment can also be used to examine the effect of such parameters as the accuracies of h/k, surface temperature, among others. To calibrate the infrared scanner in making temperature measurements, a Continuous-temperature Infrared Calibrator (CIC) has been built by this author, which is strictly designed for this purpose [25].

APPENDIX A

A SUPERPOSITION SOLUTION OF HEAT CONDUCTION IN A CAVITIED REGION SUBJECTED TO A CONVECTIVE BOUNDARY CONDITION

Introduction

The classical methods of the solution of two-dimensional boundary value problems having irregular boundaries have been limited primarily to the conformal mapping or the Schwarz iterative method. In the former method, the use of the Schwarz-Christoffel transformation permits the conversion of the problem in its original complex plane into a semi-infinite space of another complex plane. By judicious use of the proper location of the origin, scale and orientation, the problem can be transformed such that either a Fourier transform or a Poisson's integral can be applied for solution in the new problem. The method has been used in the solution of a wide range of problems [28-30].

Less well-known and yet slightly more difficult to use is the circle-to-circle mapping which permits a transformation of the regions of interest to the inside of a unit circle. Applications of this method have been found in the transformation of square bars and trochoidal cross sections [31]. On th other hand, the Schwarz iterative method follows a totally different approach. This method splits the region into overlapped sub-regions for which the exact solutions are available. Then by successively iterating and matching the temperatures inside the overlapped region, the temperature in the entire region can also be obtained. The method is useful to solve either elliptic or parabolic differential equations [32,33].

It is significant to note that the classical methods given above are only useful in the solution of the Dirichlet and the Neumann problems. The Schwarz-Christoffel transformation is still useful to solve solidification or melting problems in an irregular region provided that the

convective coefficient and the ambient temperature are treated as constants [34]. In fact, this type of problem has a constant surface temperature and therefore leads to a non-homogeneous Neumann problem. Drastically different, however, is the case if a problem has a convective boundary without phase transitions, in which case the problem becomes the combination of the Dirichlet and the Neumann problems. Then the Schwarz iterative method becomes futile; the conformal mapping technique also becomes useless because of the presence of the convective boundary condition which, in itself, presents as an unknown in the solution.

In engineering practice, heat transfer often takes place in irregular regions. In nondestructive testing, the surface temperatures can be used as clues to predict material defects [8,21,35]. In such an application the erosion of material on one side of the surfaces gives rise to an irregular inner boundary, and the outer surface dissipates heat by convection. To be able to predict surface temperatures in this instance is important to the prediction of flaws. In the present study, a superposition technique is attempted for solution. The problem under study consists of a two dimensional system with an indentation in the form of a rectangular, a circular, an elliptical or a triangular cavity on one surface; the temperature is specified on this surface. The other surface is flat and dissipates heat by convection. It will be shown that the effective thickness used in the solution has a marked effect on the prediction results. The developed solution provides an estimation of the surface temperature of systems having medium-sized cavities.

Analysis

The system under investigation is depicted in Fig. 20. A cavity is located at the origin of the coordinates. For the cavity location chosen, the y axis can be taken as the plane of symmetry. The dimension of the system in the x direction is large to the extent that the temperature gradient along the x direction vanishes at x = L. A steady state system having an arbitrary cavity configuration f(x) is chosen for analysis. The governing equation and boundary conditions pertinent to the problem can be written as follows:

Governing equation

$$\nabla^2 T=0 \tag{38}$$

Boundary conditions

$$T(x,y_o)=T_b \tag{39}$$

$$-k\frac{\partial T(x,\ell-s)}{\partial y} = h[T(x,\ell-s)-T_\infty] \tag{40}$$

$$\frac{\partial T(0,y)}{\partial x} = \frac{\partial T(L,y)}{\partial x} = 0 \tag{41}$$

where y_o represents the lower boundary, $y_o = f(x)$.

To remove the nonhomogeneity caused by the convective condition, all temperatures are measured in excess of T_∞. The problem can be normalized by introducing the dimensionless groups:

$$\theta(\xi,\eta) = \frac{T(x,y)-T_\infty}{T_b-T_\infty}\ ,\quad \xi = \frac{x}{\ell-s}\ ,\quad \eta = \frac{y}{\ell-s}$$

$$\gamma = \frac{L}{\ell-s}\ ,\quad Bi_{(\ell-s)} = \frac{h(\ell-s)}{k} \tag{42}$$

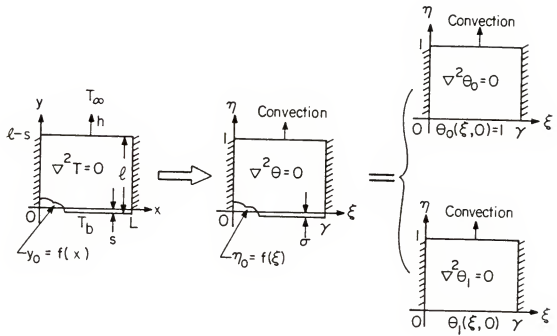

Figure 20

System for Analysis

thus yields,

Governing equation

$$\nabla^2\theta = 0 \tag{43}$$

Boundary conditions

$$\theta(\xi,\eta_o) = 1 \tag{44}$$

$$\frac{\partial\theta(\xi,1)}{\partial\eta} = -Bi_{(\ell-s)}\ \theta(\xi,1) \tag{45}$$

$$\frac{\partial\theta(0,\eta)}{\partial\xi} = \frac{\partial\theta(\gamma,\eta)}{\partial\xi} = 0 \tag{46}$$

where η_o represents the lower boundary in the normalized problem, $\eta_o = f(\xi)$. $Bi_{(\ell-s)}$ is the Biot number.

A superposition technique is used to write the solution as the sum of two functions $\theta_o(\xi,\eta)$ and $\theta_1(\xi,\eta)$ both having regular boundaries as follows (see Fig. 20).

$$\theta(\xi,\eta) = \theta_o(\xi,\eta) + \theta_1(\xi,\eta) \tag{47}$$

Now the problem boils down to the development of boundary conditions for the subproblems.

For the adiabatic condition prevailing at $\xi = 0$ and γ in the original irregular problem, the conditions for these boundaries in the regular problem can be obtained by substituting equation (47) into (46), giving,

$$\frac{\partial\theta_o(0,\eta)}{\partial\xi} = \frac{\partial\theta_o(\gamma,\eta)}{\partial\xi} = 0 \tag{48}$$

and,

$$\frac{\partial\theta_1(0,\eta)}{\partial\xi} = \frac{\partial\theta_1(\gamma,\eta)}{\partial\xi} = 0 \tag{49}$$

for $1 \geq \eta \geq 0$.

Substituting equation (47) into (44) for the irregular boundary results in ,

$$\theta(\xi,\eta_o)=1=\theta_o(\xi,\eta_o)+\theta_1(\xi,\eta_o) \tag{50}$$

in which $\theta_o(\xi,\eta_o)$ can be expanded using Taylor's series as,

$$\theta_o(\xi,\eta_o)=\theta_o(\xi,0)+\frac{\partial\theta_o(\xi,0)}{\partial\eta}\, f(\xi) \tag{51}$$

$\theta_1(\xi,\eta_o)$ can be expanded in a similar fashion; but, for convenience, only the first term of the expansion is retained (this expansion will be further examined later).

$$\theta_1(\xi,\eta_o)=\theta_1(\xi,0) \tag{52}$$

Substituting equations (51) and (52) into (50) permits a split of the resulting equation into the following two:

$$\theta_o(\xi,0)=1 \tag{53}$$

$$\frac{\partial\theta_o(\xi,0)}{\partial\eta}\, f(\xi)+\theta_1(\xi,0)=0 \tag{54}$$

Here equation (53) is the boundary condition for θ_o at $\eta = 0$. According to equation (54), the boundary condition θ_1 at the lower boundary depends on $\partial\theta_o(\xi,0)/\partial\eta$. θ_o must therefore be solved first before $\theta_1(\xi,0)$ can be formulated. For θ_o, only the boundary condition at the upper boundary is still missing, and this is found be substituting equation (47) into (45) and again splitting the resulting equation into two equations as follows.

$$\frac{\partial\theta_o(\xi,1)}{\partial\eta} = -Bi_{(\ell-s)}\,\theta_o(\xi,1) \tag{55}$$

and

$$\frac{\partial\theta_1(\xi,1)}{\partial\eta} = -Bi_{(\ell-s)}\theta_1(\xi,1) \tag{56}$$

which give the boundary conditions for the upper boundaries in both regular problems. The formulation for $\theta_o(\xi,\eta)$ is now complete; its solution can be derived as,

$$\theta_o(\xi,\eta) = 1 - \frac{Bi_{(\ell-s)}\eta}{1+Bi_{(\ell-s)}} \tag{57}$$

which is a linear function of η.

With θ_o solved, to find $\theta_1(\xi,\eta)$ is straightforward. Substituting equation (57) into (54) gives the boundary condition for θ_1 at the lower boundary as,

$$\theta_1(\xi,0) = \frac{Bi_{(\ell-s)}}{1 + Bi_{(\ell-s)}} f(\xi) \tag{58}$$

The boundary conditions (equations (49), (56), and (58)) for problem $\theta_1(\xi,\eta)$ are now complete and the solution is given as follows.

$$\theta_1 = E_o + \sum_{n=1}^{\infty} E_n \cos\lambda_n\xi \frac{\cosh\lambda_n(1-\eta) + \frac{Bi_{(\ell-s)}}{\lambda_n}\sinh\lambda_n(1-\eta)}{\cosh\lambda_n + \frac{Bi_{(\ell-s)}}{\lambda_n}\sinh\lambda_n} \tag{59}$$

where $\lambda_n = \frac{n\pi}{\gamma}$, n=1, 2, ...

and,

$$E_o = \frac{Bi_{(\ell-s)}}{(1+Bi_{(\ell-s)})} \int_o^{\gamma} f(\xi)\,d\xi \tag{60}$$

$$E_n = \frac{2Bi_{(\ell-s)}}{\gamma(1+Bi_{(\ell-s)})} \int_o^{\gamma} f(\xi)\cos\lambda_n\xi\,d\xi \tag{61}$$

Using this general formulation as basis, one can specialize the solution to four cavity configurations as shown in Fig. 21. For the rectangular cavity (Fig. 21(a)), the irregular boundary can be expressed as,

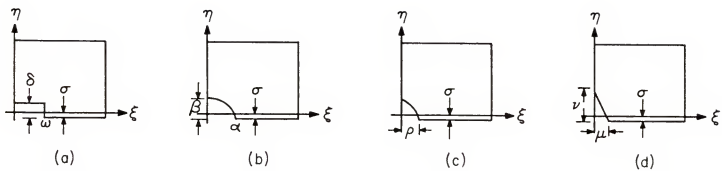

Figure 21

Notations for Cavities

$$f(\xi) = \begin{cases} \delta-\sigma & \text{for } \omega \geq \xi \geq 0 \\ -\sigma & \text{for } \gamma \geq \xi \geq \omega \end{cases} \tag{62}$$

where,

$$\delta = \frac{d}{\ell-s} \ , \ \sigma = \frac{s}{\ell-s} \ , \ \omega = \frac{w}{\ell-s}$$

and w and d refer to width and depth of the cavity in x and y directions, respectively in the original problem.

For the elliptical cavity (Fig. 21(b)),

$$f(\xi) = \begin{cases} -\sigma + \beta \left[1 - \left(\frac{\xi}{\alpha}\right)^2\right]^{\frac{1}{2}} & \text{for } \alpha \geq \xi \geq 0 \\ -\sigma & \text{for } \gamma \geq \xi \geq \alpha \end{cases} \tag{63}$$

where $\alpha = \frac{a}{\ell-s}$, $\beta = \frac{b}{\ell-s}$

and a and b refer to major and minor axes of the cavity in x and y directions, respectively.

A special case of the elliptical cavity is the circular cavity (Fig. 21(c)), for which,

$$f(\xi) = \begin{cases} -\sigma + \rho \left[1 - \left(\frac{\xi}{\rho}\right)^2\right]^{\frac{1}{2}} & \text{for } \rho \geq \xi \geq 0 \\ -\sigma & \text{for } \gamma \geq \xi \geq \rho \end{cases} \tag{64}$$

where $\rho = \frac{r_o}{\ell-s}$ is the dimensionless radius of the cavity.

Finally, for the triangular cavity (Fig. 21(d)),

$$f(\xi) = \begin{cases} -\sigma + \nu \left(1 - \frac{\xi}{\mu}\right) & \text{for } \mu \geq \xi \geq 0 \\ -\sigma & \text{for } \gamma \geq \xi \geq \mu \end{cases} \tag{65}$$

where $\mu = \frac{u}{\ell-s}$, $\nu = \frac{v}{\ell-s}$

and u and v refer to opening and depth of the triangular cavity in x and y directions, respectively.

Substituting equation (62) into equation (60) and (61) results in,

$$E_o = \frac{Bi_{(\ell-s)}}{\gamma(1+Bi_{(\ell-s)})} \ (\delta\omega-\sigma\gamma) \tag{66}$$

$$E_n = \frac{2Bi_{(\ell-s)}}{\gamma(1+Bi_{(\ell-s)})} \ \frac{\delta}{\lambda_n} \sin\lambda_n\omega \tag{67}$$

which are valid for a rectangular cavity. In a similar manner E_o and E_n can be divided for elliptical, circular and triangular cavities and expressed respectively as,

$$E_o = \frac{Bi_{(\ell-s)}}{\gamma(1+Bi_{(\ell-s)})} \ (\frac{\pi}{4}\alpha\beta-\sigma\gamma) \tag{68}$$

$$E_n = \frac{2Bi_{(\ell-s)}}{\gamma(1+Bi_{(\ell-s)})} \ \beta \int_o^{\alpha} [1-(\frac{\xi}{\alpha})^2]^{\frac{1}{2}} \cos\gamma_n\xi \, d\xi \tag{69}$$

$$E_o = \frac{Bi_{(\ell-s)}}{\gamma(1+Bi_{(\ell-s)})} \ (\frac{\pi}{4}\rho^2-\sigma\gamma) \tag{70}$$

$$E_n = \frac{2Bi_{(\ell-s)}}{\gamma(1+Bi_{(\ell-s)})} \ \rho \int_o^{\rho} [1-(\frac{\xi}{\rho})^2]^{\frac{1}{2}} \cos\lambda_n\xi \, d\xi \tag{71}$$

and,

$$E_o = \frac{Bi_{(\ell-s)}}{\gamma(1+Bi_{(\ell-s)})} \ (\frac{1}{2}\mu\nu-\sigma\gamma) \tag{72}$$

$$E_n = \frac{2Bi_{(\ell-s)}}{\gamma(1+Bi_{(\ell-s)})} \ \frac{\nu}{\mu} \frac{1}{\lambda_n^2} (1-\cos\lambda_n\mu) \tag{73}$$

The desired temperature distributions can now be obtained by substituting equations (66) and (73) into equation (59) which is, in turn, substituted together with equation (57) into equation (47) to obtain the final solution. Because of the presence of oscillatory functions in equations (69) and (71), the Filon Formula must be used to evaluate integrals in these equations.

Critique

A careful examination of the solution presented above reveals that the proposed superposition technique bears close resemblance to the perturbation solution. Indeed, if an ordering parameter ϵ is used as a multiplying factor for $\theta_1(\xi,\eta)$ term in equation (47), the desired temperature is expanded to the first order of the ordering parameter. In the expansion of $\theta_o(\xi,\eta)$ into Taylor's series in equation (51) the expansion is terminated at $\partial\theta_o(\xi,0)/\partial\eta$. Hence, this expansion is also developed to the same order. On the other hand, in the expansion of $\theta_1(\xi,\eta_o)$ only the first term is retained, see equation (52). This arbitrariness is borne out of the fact that, since the $\theta_1(\xi,\eta_o)$ term in equation (50) will also be multiplied by ϵ in the perturbation method, omission of $\partial\theta_1(\xi,0)/\partial\eta$ term corresponds to the exclusion of ϵ^2 term in the final expansion, which is valid for $\epsilon<1$. It is also noted that the grouping of terms in equations (53) and (54) is actually suggested by the perturbation method in which terms of the same order of magnitude are equated to develop these relations.

The division of the original problem into two subproblems is meaningful from the physical standpoint. According to the perturbation method, the term $\theta_o(\xi,\eta)$ represents the unperturbed part of the solution. In the present problem, because of the adiabatic edges, this leads to a one-dimensional problem. Equation (57) is the solution to this unperturbed problem and the equation represents how the temperature would distribute in the system if the cavity is missing. The second term $\theta_1(\xi,\eta)$, according to the perturbation method, represents the perturbed solution. Here the problem is a boundary perturbation [37] and $\theta_1(\xi,\eta)$ modifies the temperature distribution to demonstrate the cavity effect. In more specific

terms, if heat flow in Fig. 20 is pointed upward, the perturbed part of the solution will give rise to a hot spot located at $\xi = 0$. Moving toward the edges ($\xi=\gamma$), the temperature in the system should reach asymptotically that of a plane slab as though the cavity is not there. In fact, the overall temperature level for θ_1 is modulated by a constant bias represented by the unperturbed part of the solution (θ_o).

It is well-known in applied mathematics that the perturbation solution is only valid for small perturbations which, in the present application, refer to small cavities. For a small perturbation the ordering parameter $\varepsilon<1$, which makes it justified to expand θ_o and θ_1 according to equations (51) and (52). The solution of problems having a small perturbation has been well developed and is of no concern to this study.

For medium-sized cavities, the perturbation solution is generally considered to be useless. In fact, tests conducted in this study indicate that, if the perturbation solution had been useful, the ordering parameter would have taken a value close to unity (this point will be further examined in the next section) and, as such, equations (51) and (52) would have to be expanded to higher orders to be mathematically rigorous. However, by expanding functions to higher orders, one will eventually obtain a Fourier series solution whose coefficients can no longer be solved using the orthogonality relationship.

Fortunately, in the present work, there is a parameter similicity contained in several dimensionless groups in the solution. This parameter has the effect of moving ξ axis upward (see Fig. 20) such that the expansion of θ_1 about the original ξ axis is replaced by an expansion of this function about a pseudo mean function. While this replacement provides the justification to delete higher order terms in the

expansion, it also makes the solution approximate. Attention is now directed to the evaluation of this s and the method used to substitute the final solution into the governing equation and the boundary conditions.

As it turned out, both equations (43) and (46) are identically satisfied by the solution. In order to satisfy equation (45), the following conditions must be met:

$$s = \frac{dw}{L} \tag{74}$$

$$s = \frac{\pi ab}{4L} \tag{75}$$

$$s = \frac{\pi r_o^2}{4L} \tag{76}$$

$$s = \frac{uv}{2L} \tag{77}$$

which are valid for rectangular, elliptical, circular and triangular cavities, respectively. These equations can all be converted to a general form as follows.

$$s = \frac{\text{cross-sectional area of the cavity } (A_c)}{L} \tag{78}$$

Amazingly, this equation is exactly what one would expect from a purely geometrical standpoint. Finally, substituting the solution into equation (44) yields,

$$-\frac{Bi(\ell-s)\eta_o}{1+Bi(\ell-s)} + E_o + \sum_{n=1}^{\infty} E_n \cos\lambda_n\xi \; \frac{\cosh\lambda_n(1-\eta_o) + \frac{Bi(\ell-s)}{\lambda_n}\sinh\lambda_n(1-\eta_o)}{\cosh\lambda_n + \frac{Bi(\ell-s)}{\lambda_n}\sinh\lambda_n} = 0 \tag{79}$$

where equation (78) has been used for simplification. Unfortunately, the final solution is unable to satisfy the boundary condition.

Results and Discussion

It remains to be seen if the approximate solution developed above is truly useful to estimate temperatures as desired; this can only be verified by using data as demonstrated as follows.

In this work the true temperatures were obtained by using a numerical solution. Next, the approximate solution developed in this study was used to predict temperatures, and these temperatures were compared with the true temperatures computed earlier. A sample test is shown in Fig. 22. Some observations can be made from this figure.

There are two sets of data plotted for the predicted temperatures in this figure. The one identified with s=0 shows how data behave when the ξ axis is not shifted upward, an over-prediction of 11 to 16% for $x/L = 0$ to 1. If the axis is shifted according to equation (78) and this shift is accounted for in the solution, the predicted data agree with the true temperature satisfactorily at $x/L = 0$. Nevertheless, a slight overprediction of 1.3% is still observed at $x/L = 1$, but the improvement is remarkable.

Next the amplitude of the temperature curves will be examined and this serves to explain why the superposition is written as equation (47). As it is shown in the figure, there is a 0.033 drop in the true surface temperature from $x/L = 0$ to 1; the corresponding drop in the predicted temperature is 0.026. Recall that it is the perturbed part of the solution that gives rise to the x dependency; then, if the ordering parameter had been used in the superposition, this parameter would have taken a value of 1.269 which would be in contradiction to the role it plays in the original

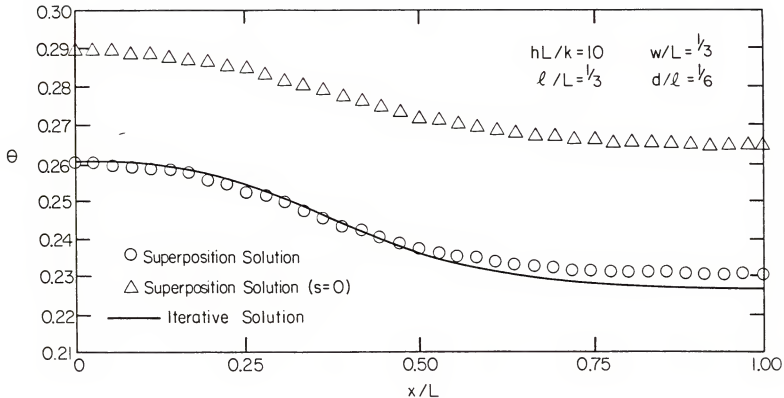

Figure 22

Comparison Between the True and Predicted Temperatures
Based on an Approximate Solution

perturbation solution. The overall temperature levels appear to be more important and this explains why ε is not used as a parameter in the present solution.

Based on the good results obtained, a massive computation was launched to evaluate surface temperatures for thirty-six cases as tabulated in Table 2. The approximate solution was also used to generate a large body of predicted temperatures; in this computation, the parameter ε was treated as a variable. The analyzed s values given in the table represent those which offer a best matching between the predicted and the true temperatures. Finally, equation (78) was used to predict this s value and the result is listed in the last column. The agreement between the analyzed and predicted s is good for most cases tested. In order to facilitate viewing, these data are also plotted as shown in Fig. 23.

It is noted that the approximate solution given in this work is not able to predict the interior temperatures as well as it is done on the surface; the prediction worsens moving closer to the cavity. Also, because of the difficulties involved in dealing with irregular boundaries in the numerical solution, prediction equations for other cavity configurations (elliptical, circular or triangular) were not tested in this study.

Table 2

Comparison Between Predicted and Analyzed s
for Systems Having Rectangular Cavities

			Analyzed s			Predicted s
			Biot Number = hL/k			$s=\frac{A_c}{L^2}$
$\frac{\ell}{L}$	$\frac{w}{L}$	$\frac{d}{\ell}$	5	10	13	
$\frac{1}{3}$	$\frac{1}{12}$	$\frac{1}{12}$	0.05	0.05	0.08	0.08
		$\frac{1}{6}$	0.08	0.07	0.08	
	$\frac{1}{6}$	$\frac{1}{12}$	0.13	0.16	0.16	0.17
		$\frac{1}{6}$	0.15	0.16	0.17	
	$\frac{1}{3}$	$\frac{1}{12}$	0.33	0.31	0.33	0.33
		$\frac{1}{6}$	0.30	0.33	0.33	
$\frac{1}{2}$	$\frac{1}{12}$	$\frac{1}{18}$	0.08	0.08	0.08	0.08
		$\frac{1}{9}$	0.08	0.08	0.08	
	$\frac{1}{6}$	$\frac{1}{18}$	0.16	0.16	0.17	0.17
		$\frac{1}{9}$	0.16	0.16	0.17	
	$\frac{1}{3}$	$\frac{1}{18}$	0.35	0.33	0.34	0.33
		$\frac{1}{9}$	0.35	0.33	0.34	

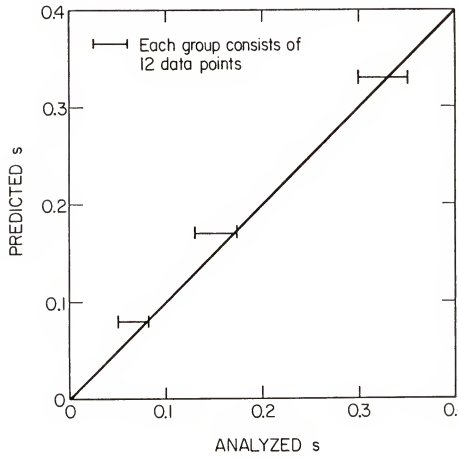

Figure 23

Correlation Between Predicted and Analyzed s

APPENDIX B

COMPUTER PROGRAM FOR COMPUTATION OF SURFACE TEMPERATURES ON A PLANE WALL HAVING A PRESCRIBED CAVITY GEOMETRY, THE LOWER BOUNDARY HAVING A SPECIFIED TEMPERATURE

Table 3

Definitions of Input Variables for the Program Given in Appendix B

Variable Name	Definition
NI*	Number of nodal points in the I-direction
NJ	Number of nodal points in the J-direction
MI	Location of cavity boundary in the I-direction
MJ	Location of cavity boundary in the J-direction
TT	$(T-T_A)/(T_B-T_A)$ evaluated at the lower boundary, i.e. $(T_B-T_A)/(T_B-T_A)=1$
TA	$(T_A-T_A)/(T_B-T_A)=0$ in this program
DL	Number of intervals in the J-direction
EPS	Convergence criterion for iteration
HK	=hL/k, Biot number, where h is convective heat transfer coefficient, L is system length, k is thermal conductivity
DEL+	$=1/DL=\Delta x/L=\Delta y/L$, mesh size

*Refer to Figure 24 for nodal locations.
+Square meshes are used in this computer program.

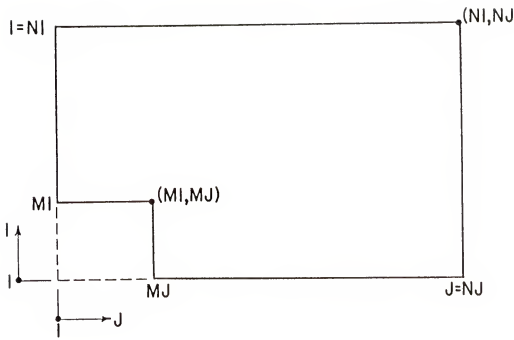

Figure 24

A Schematic Diagram Showing Nodal Locations
Used in the Computer Program Given in Appendix B

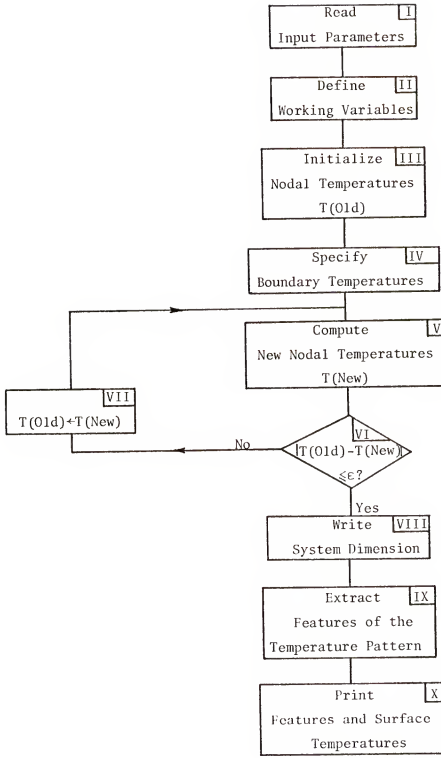

Figure 25

Block Diagram Showing Iteration Procedures for the Computer Program Given in Appendix B

```
C
C       THIS PROGRAM EVALUATES THE SURFACE TEMPERATURE
C       NONUNIFORMITY AS A FUNCTION OF MATERIAL EROSION.
C       A TWO DIMENSIONAL MODEL IS BEING CONSIDERED. THE
C       EROSION IS MODELED USING A CAVITY OF RECTANGULAR
C       CROSS-SECTION. THE SURFACE RECEIVING HEAT IS ISO-
C       THERMAL. THE OUTER SURFACE IS A CONVECTIVE BOUN-
C       DARY. PLANES OF SYMMETRY ARE USED TO REDUCE THE
C       NUMBER OF NODES CONSIDERED.
C
        DIMENSION T(19,37),TNEW(19,37),A(37),B(37)
  I     READ (5,1) NI,NJ,MI,MJ,HK,TT,TA,EPS,DL
      1 FORMAT (4I3,5F8.5)
        DEL=1./DL
        BI=HK*DEL
        TPBI=2.+BI
 II     LI=NI-1
        LJ=NJ-1
        KI=MI+1
        KJ=MJ+1
        DO 2 I=1,NI
III     DO 2 J=1,NJ
      2 T(I,J)=(TT+TA)/2.
        DO 3 J=1,NJ
        TNEW(1,J)=TT
      3 T(1,J)=TT
 IV     DO 4  I=2,MI
        DO 4 J=1,MJ
        TNEW(I,J)=TT
      4 T(I,J)=TT
     20 DO 5  I=KI,LI
      5 TNEW(I,1)=(T(I-1,1)+T(I+1,1)+2.*T(I,2))/4.
        DO 6  I=2,LI
      6 TNEW(I,NJ)=(T(I-1,NJ)+T(I+1,NJ)+2.*T(I,NJ-1))/4.
        IF (LJ .EQ. MJ) GO TO 60
        DO 8  I=2,MI
        DO 8  J=KJ,LJ
      8 TNEW(I,J)=(T(I-1,J)+T(I+1,J)+T(I,J-1)+T(I,J+1))/4.
     60 DO 9  I=KI,LI
        DO 9  J=2,LJ
  V   9 TNEW(I,J)=(T(I-1,J)+T(I+1,J)+T(I,J-1)+T(I,J+1))/4.
        DO 7 J=2,LJ
      7 TNEW(NI,J)=(T(LI,J)+(T(NI,J-1)+T(NI,J+1))/2.+BI*TA)/TPBI
        TNEW(NI,1)=(T(LI,1)+T(NI,2)+BI*TA)/TPBI
        TNEW(NI,NJ)=(T(LI,NJ)+T(NI,LJ)+BI*TA)/TPBI
        DO 10 I=2,MI
        DO 10 J=KJ,NJ
        IF (ABS(T(I,J)-TNEW(I,J))-EPS) 10,10,15
     10 CONTINUE
        DO 11 I=KI,NI
        DO 11 J=1,NJ
 VI     IF (ABS(T(I,J)-TNEW(I,J))-EPS) 11,11,15
```

```
   11 CONTINUE
      GO TO 90
   15 DO 16 I=2,MI
      DO 16 J=KJ,NJ
VII 16 T(I,J)=TNEW(I,J)
      DO 17 I=KI,NI
      DO 17 J=1,NJ
   17 T(I,J)=TNEW(I,J)
      GO TO 20
   90 XMI=MI
      YMJ=MJ
      DEPTH=(XMI-1.)/36.
      ACROS=(YMJ-1.)/36.
      XNI=NI
      YNJ=NJ
VIII  THICK=(XNI-1.)/36.
      WIDTH=(YNJ-1.)/36.
      WRITE (6,12) THICK,WIDTH,DEPTH,ACROS
   12 FORMAT (1H0,32HREFRACTORY DIMENSION: THICKNESS=,F6.2,
     / 12H,HALF WIDTH=,F6.2,15H ;CAVITY DEPTH=,F6.4,
     / 12H,HALF WIDTH=,F6.4,3HIN.)
      WRITE (6,39) HK,THICK,WIDTH,DEPTH,ACROS,NI,NJ,TT,TA,EPS
   39 FORMAT (5F8.4, 2I3, 3F8.5)
      PUNCH 35,    HK,THICK,WIDTH,DEPTH,ACROS,NI,NJ,TT,TA,EPS
   35 FORMAT (5F8.4, 2I3, 3F8.5)
      NA=NJ-1
      DO 30 J=1,NA
   30 A(J)=TNEW(NI,J)-TNEW(NI,J+1)
      CALL MAXSLP(A,NA,TFL,IP)
      POS=IP
      PINFL=(POS-0.5)*DEL
      TINFL= (TNEW(NI,IP)+TNEW(NI,IP+1))/2.
      AREA1=0.
      AREA2=0.
      AREA3=AREA4=AREA5=AREA6=0.
      DO 31 J=2,IP
   31 AREA1=AREA1+((TNEW(NI,J)+TNEW(NI,J-1))/2.-TINFL)*DEL
      AREA1=AREA1+(TNEW(NI,IP)-TINFL)/2.*DEL
      IPA=IP+1
      DO 32 J=IPA,NA
   32 AREA2=AREA2+(TINFL-(TNEW(NI,J)+TNEW(NI,J+1))/2.)*DEL
      AREA2=AREA2+(TINFL-TNEW(NI,IPA))/2.*DEL
      IPB=IP-4
      IPC=IPA+4
IX    IPD=IPC+4
      IPE=IPD+4
      IF (IPB .LE. 1)  GO TO 50
      DO 41 J=IPB,IP
   41 AREA3=AREA3+((TNEW(NI,J)+TNEW(NI,J-1))/2.-TINFL)*DEL
      AREA3=AREA3+(TNEW(NI,IP)-TINFL)/2.*DEL
   50 IF (IPC .GE. NJ) GO TO 51
      IPC1=IPC-1
```

```
      DO 42 J=IPA,IPC1
   42 AREA4=AREA4+(TINFL-(TNEW(NI,J)+TNEW(NI,J+1))/2.)*DEL
      AREA4=AREA4+(TINFL-TNEW(NI,IPA))/2.*DEL
      IF (IPD .GE. NJ) GO TO 51
      IPD1=IPD-1
      DO 43 J=IPC,IPD1
   43 AREA5=AREA5+(TINFL-(TNEW(NI,J)+TNEW(NI,J+1))/2.)*DEL
      IF (IPE .GE. NJ) GO TO 51
      IPE1=IPE-1
      DO 44 J=IPD, IPE1
   44 AREA6=AREA6+(TINFL-(TNEW(NI,J)+TNEW(NI,J+1))/2.)*DEL
      GO TO 53
   51 WRITE (6,52)
   52 FORMAT (5X,31HVALUE(S) EXCEED RANGE OF DOMAIN//)
   53 WRITE (6,33) TNEW(NI,1),TNEW(NI,NJ),PINFL,AREA1,AREA2
     /           ,AREA3,AREA4,AREA5,AREA6
   33 FORMAT (5X,25HMAXIMUM TEMPERATURE IS T=,F10.5/
     /        5X,25HMINIMUM TEMPERATURE IS T=,F10.5/
     /        5X,27HPOINT OF INFLECTION AT X/L=,F10.5/
     /        5X,27HAREA ABOVE INFLECTION TEMP=,F10.5/
     /        5X,27HAREA BELOW INFLECTION TEMP=,F10.5/
     /        5X,6HAREA3=,F10.5/5X,6HAREA4=,F10.5/5X,6HAREA5=,
X    /        F10.5/5X,6HAREA6=,F10.5)
      WRITE (6,34) (TNEW(NI,J),J=1,NJ)
   34 FORMAT (1H0,5(/8F10.7))
      PUNCH 36, TNEW(NI,1),TNEW(NI,NJ),PINFL,AREA1,AREA2
     /        ,AREA3,AREA4,AREA5,AREA6
   36 FORMAT (9F8.5)
      PUNCH 37, (TNEW(NI,J), J=1,NJ)
   37 FORMAT (8F10.7)
      STOP
      END
      SUBROUTINE MAXSLP(B,N,VAL,IO)
      DIMENSION B(37)
      VAL=0.
      IO=0
      DO 1 I=1,N
      IF (B(I) .LE. VAL) GO TO 1
      VAL=B(I)
      IO=I
    1 CONTINUE
      RETURN
      END
```

APPENDIX C

COMPUTER PROGRAM TO PREDICT CAVITY GEOMETRY FOR THE SYSTEM GIVEN IN APPENDIX B

Table 4

Definitions of Additional Input Variables for the Program given in Appendix C

Variable Name[+]	Definition
DLT	$\left\|T_{calculated}-T_{measured}\right\|$, a specified criterion used to determine the location of cavity (side) wall
EPS1	$\left\|T_{calculated}-T_{measured}\right\|$, a specified criterion used to determine the location of cavity top
AAA[*]	Alphameric variable used to identify input data set
DSL[*]	$=d/\ell$, true dimensionless cavity depth read into computer for print-out and comparison
WL[*]	$=w/L$, true dimensionless cavity depth read into computer for print-out and comparison
PINFL[*]	True position of the inflection point extracted from the input surface temperature
T1	Surface temperature (variable)

[+]This table is to be used together with Table 3 for definitions of all input variables.

[*]These variables are not necessary to run this program.

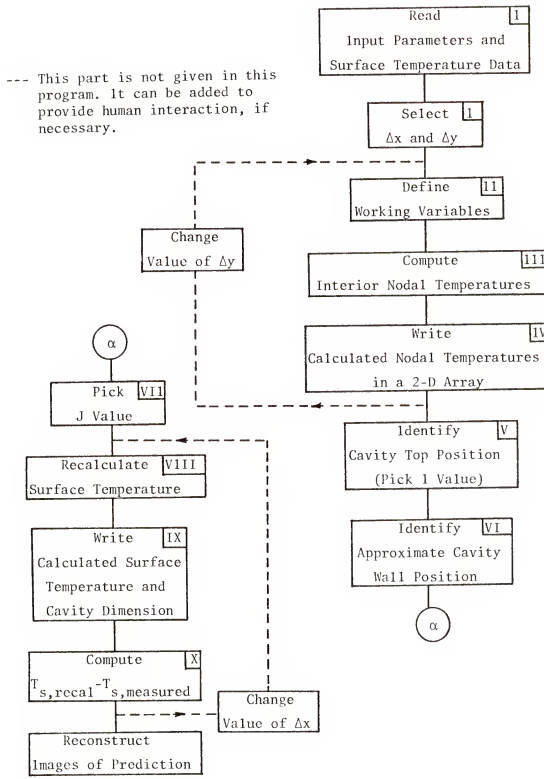

Figure 26

Block Diagram for the Computer Program Given in Appendix C

```
C
C ******************************************************
C *   THIS PROGRAM PREDICTS POSSIBLE CAVITY SIZE WITH    *
C *   GIVEN SURFACE TEMPERATURE DISTRIBUTION. DATA SMOOTH*
C *   ROUTINE(1-6-1) APPLIED ON CALCULATED VALUES. CAVITY*
C *   SIDE HAS PRESCRIBED SURFACE TEMPERATURE.           *
C ******************************************************
C
      DIMENSION T(13, 37),T1(37),T2(37),T3(13,37),AAA(4)
     /          ,TNEW(13,37)
      READ (5,101) NI,NJ,TA,TT,EPS,DL,DLT,EPS1
  101 FORMAT (2I3,6F8.5)
      DEL=1./DL
      LI=NI-1
I     LJ=NJ-1
      READ (5,501) AAA
  501 FORMAT (4A4)
      READ (5,102) HK,DSL,WL,PINFL,(T1(I),I=1,NJ)
  102 FORMAT (F8.4,16X,2F8.4/16X,F8.5/(8F10.7))
      WRITE (6,502) AAA
  502 FORMAT (1H1,///2X,4A4)
      WRITE (6,103) HK,DSL,WL,PINFL
  103 FORMAT (1H0,4F10.4)
      WRITE(6,503) (T1(I),I=1,NJ)
  503 FORMAT(8F10.7)
      DYX=1.
II    BI=DYX*HK*DEL
      DYX2=DYX**2
      TPBI=1.+DYX2+BI
      CI=1.+DYX2
      DO 400 J=1,NJ
  400 T2(J)=T1(J)
      DO 200 J=1,NJ
      T(NI,J)=T2(J)
  200 T3(NI,J)=T(NI,J)
      T(NI-1,1)=T(NI,1)*TPBI-T(NI,2)*DYX2-TA*BI
      DO 201 J=2,LJ
  201 T(NI-1,J)=T(NI,J)*TPBI-(T(NI,J-1)+T(NI,J+1))/2.*DYX2
     /          -TA*BI
      T(NI-1,NJ)=T(NI,NJ)*TPBI-T(NI,LJ)*DYX2-TA*BI
III   T3(NI-1,1)=(6.*T(NI-1,1)+2.*T(NI-1,2))/8.
      DO 401 J=2,LJ
  401 T3(NI-1,J)=(T(NI-1,J-1)+6.*T(NI-1,J)+T(NI-1,J+1))/8.
      T3(NI-1,NJ)=(2.*T(NI-1,LJ)+6.*T(NI-1,NJ))/8.
      DO 260 J=1,NJ
  260 T(NI-1,J)=T3(NI-1,J)
      DO 202 I=2,LI
      T(NI-I,1)=T(NI-I+1,1)*2.*CI-T(NI-I+1,2)*2.*DYX2
     /          -T(NI-I+2,1)
      T(NI-I,NJ)=T(NI-I+1,NJ)*2.*CI-T(NI-I+1,LJ)*2.*DYX2
     /          -T(NI-I+2,NJ)
      DO 410 K=2,LJ
```

```
      J=LJ-K+2
  410 T(NI-I,J)=T(NI-I+1,J)*2.*CI-T(NI-I+1,J-1)*DYX2
     /       -T(NI-I+1,J+1)
     /              *DYX2-T(NI-I+2,J)
      T3(NI-I,1)=(6.*T(NI-I,1)+2.*T(NI-I,2))/8.
      DO 403 L=2,LJ
  403 T3(NI-I,L)=(T(NI-I,L-1)+6.*T(NI-I,L)+T(NI-I,L+1))/8.
      T3(NI-I,NJ)=(2.*T(NI-I,LJ)+6.*T(NI-I,NJ))/8.
      DO 405 L=1,NJ
  405 T(NI-I,L)=T3(NI-I,L)
  202 CONTINUE
      DO 206 I=1,NI
      ND=NI-I+1
IV    WRITE (6,210) ND
  210 FORMAT (1H ,I4)
      WRITE (6,207) (T3(ND,J),J=1,NJ)
  207 FORMAT (5X,8F10.7)
  206 CONTINUE
      DLT=0.01
      DO 105 I=1,NI
 V    ND=NI-I+1
      IF(ABS(T3(ND,1)-1.) .LT. EPS1) GO TO 106
  105 CONTINUE
  106 I1=ND
      DO 107 J=1,NJ
VI    IF(ABS(T3(I1,J)-1.) .GT. DLT) GO TO 108
  107 CONTINUE
  108 J1=J
C
C
      MI=I1
      J3=J1+2
VII   DO 91 MJ=J1,J3
      KI=MI+1
      KJ=MJ+1
      DO 2 I=1,NI
      DO 2 J=1,NJ
    2 T(I,J)=(TT+TA)/2.
      DO 3 J=1,NJ
      TNEW(1,J)=TT
    3 T(1,J)=TT
      DO 4  I=2,MI
VIII  DO 4 J=1,MJ
      TNEW(I,J)=TT
    4 T(I,J)=TT
   20 DO 5  I=KI,LI
    5 TNEW(I,1)=(T(I-1,1)+T(I+1,1)+2.*T(I,2))/4.
      DO 6  I=2,LI
    6 TNEW(I,NJ)=(T(I-1,NJ)+T(I+1,NJ)+2.*T(I,NJ-1))/4.
      IF (LJ .EQ. MJ) GO TO 60
      DO 8  I=2,MI
      DO 8  J=KJ,LJ
```

```
    8 TNEW(I,J)=(T(I-1,J)+T(I+1,J)+T(I,J-1)+T(I,J+1))/4.
   60 DO 9  I=KI,LI
      DO 9  J=2,LJ
    9 TNEW(I,J)=(T(I-1,J)+T(I+1,J)+T(I,J-1)+T(I,J+1))/4.
      DO 7 J=2,LJ
    7 TNEW(NI,J)=(T(LI,J)+(T(NI,J-1)+T(NI,J+1))/2.+BI*TA)/TPBI
      TNEW(NI,1)=(T(LI,1)+T(NI,2)+BI*TA)/TPBI
      TNEW(NI,NJ)=(T(LI,NJ)+T(NI,LJ)+BI*TA)/TPBI
      DO 10 I=2,MI
      DO 10 J=KJ,NJ
      IF (ABS(T(I,J)-TNEW(I,J))-EPS) 10,10,15
   10 CONTINUE
VIII  DO 11 I=KI,NI
      DO 11 J=1,NJ
      IF (ABS(T(I,J)-TNEW(I,J))-EPS) 11,11,15
   11 CONTINUE
      GO TO 90
   15 DO 16 I=2,MI
      DO 16 J=KJ,NJ
   16 T(I,J)=TNEW(I,J)
      DO 17 I=KI,NI
      DO 17 J=1,NJ
   17 T(I,J)=TNEW(I,J)
      GO TO 20
   90 XMI=MI
      YMJ=MJ
      XLJ=LJ
      DEPTH=(XMI-1.)/XLJ
      ACROS=(YMJ-1.)/XLJ
      XNI=NI
 IX   YNJ=NJ
      THICK=(XNI-1.)/XLJ
      WIDTH=(YNJ-1.)/XLJ
      WRITE (6,12) THICK,WIDTH,DEPTH,ACROS
   12 FORMAT (1H0,32HREFRACTORY DIMENSION: THICKNESS=,F6.2,
     / 12H,HALF WIDTH=,F6.2,15H ;CAVITY DEPTH=,F6.4,
     / 12H,HALF WIDTH=,F6.4,3HIN.)
      WRITE(6,504) (TNEW(NI,J),J=1,NJ)
  504 FORMAT(8F10.7)
      DO 505 J=1,NJ
  505 TNEW(NI,J)=TNEW(NI,J)-T1(J)
  X   WRITE(6,504) (TNEW(NI,J),J=1,NJ)
   91 CONTINUE
      STOP
      END
```

APPENDIX D

COMPUTER PROGRAM FOR COMPUTATION OF SURFACE TEMPERATURES FOR A RECTANGULAR PARALLELEPIPED WITH A PRESCRIBED RECTANGULAR HOLE IN IT, THE HOLE BOUNDARY HAVING A SPECIFIED TEMPERATURE

Table 5

Definitions of Input Variables for the Program Given in Appendix D

Variable Name	Definition
NI*	Number of Nodal Points in I-direction
NJ	Number of Nodal Points in J-direction
MI	Location of cavity bottom boundary
MMI	Location of cavity top boundary
MJ	Location of cavity left boundary
MMJ	Location of cavity right boundary
BT	hL/k, Biot number, where h is convective heat transfer coefficient, L is system length and k is thermal conductivity
TA	$(T_A-T_A)/(T_B-T_A)=0$ in this program
TT	$(T-T_A)/(T_B-T_A)$ evaluated at the hole boundary, i.e. $(T_B-T_A)/(T_B-T_A)=1$
EPS	Convergence criterion for iteration

*Refer to Figure 27 for nodal locations. Square meshes are used in this computer program.

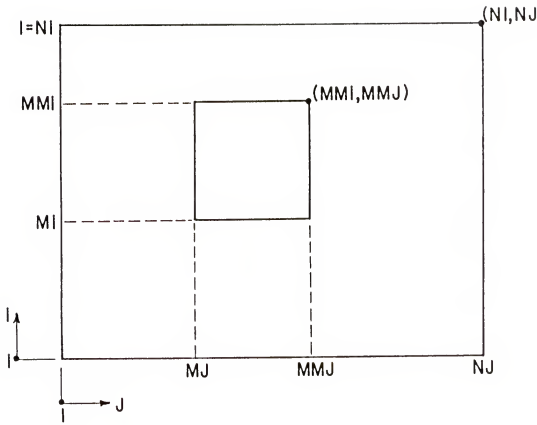

Figure 27

A Schematic Diagram Showing Nodal Locations Used in the Computer Program for a Parallelepiped

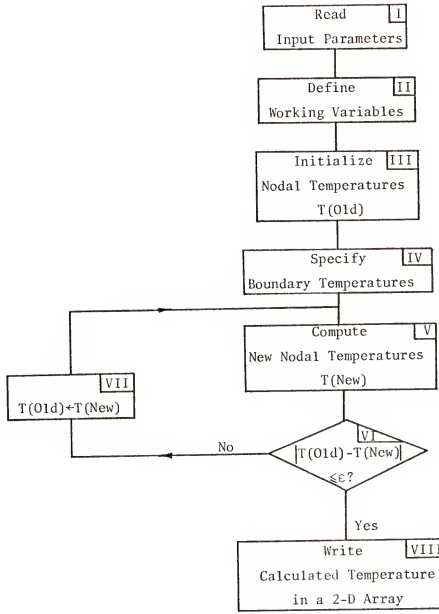

Figure 28

Block Diagram Showing Iteration Procedures for the Computer Program Given in Appendix D

```
C
C       THIS PROGRAM EVALUATES THE TEMPERATURE DISTRIBUTION
C       OF A PARALLELPIPED BLOCK WITH A RECTANGULAR CROSS-
C       SECTIONAL HOLE IN IT. THE INSIDE HOLE HAS A PRES-
C       CRIBED BOUNDARY TEMPERATURE. THE OUTSIDE SURFACE
C       IS CONVECTIVE.
C
        DIMENSION T(40,40),TNEW(40,40)
        READ (5,101) NI,NJ,MI,MJ,MMI,MMJ,BT,TA,TT,EPS
  101   FORMAT (6I3,4F8.5)
        DL=NJ-1
        DEL=1./DL
        BI=BT*DEL
        BTA=BI*TA
        TPBI=2.+BI
        TQBI=2.+2.*BI
        LI=NI-1
   II   LJ=NJ-1
        KI=MI-1
        KJ=MJ-1
        K1I=MI+1
        K1J=MJ+1
        K2I=MMI-1
        K2J=MMJ-1
        K3I=MMI+1
        K3J=MMJ+1
        DO 102 I=1,NI
  III   DO 102 J=1,NJ
  102   T(I,J)=(TT+TA)/2.
        DO 103 I=MI,MMI
        DO 103 J=MJ,MMJ
   IV   T(I,J)=TT
  103   TNEW(I,J)=TT
  200   DO 104 I=2,LI
        DO 104 J=2,KJ
  104   TNEW(I,J)=(T(I-1,J)+T(I+1,J)+T(I,J+1)+T(I,J-1))/4.
        DO 105 I=K3I,LI
        DO 105 J=MJ,MMJ
  105   TNEW(I,J)=(T(I-1,J)+T(I+1,J)+T(I,J-1)+T(I,J+1))/4.
        DO 106 I=2,LI
        DO 106 J=K3J,LJ
  106   TNEW(I,J)=(T(I-1,J)+T(I+1,J)+T(I,J-1)+T(I,J+1))/4.
        DO 107 I=2,KI
        DO 107 J=MJ,MMJ
  107   TNEW(I,J)=(T(I-1,J)+T(I+1,J)+T(I,J-1)+T(I,J+1))/4.
        DO 108 I=2,LI
  108   TNEW(I,1)=(T(I,2)+.5*(T(I+1,1)+T(I-1,1))+BTA)/TPBI
        TNEW(NI,1)=(T(LI,1)+T(NI,2)+2.*BTA)/TQBI
    V   DO 109 J=2,LJ
  109   TNEW(NI,J)=(T(LI,J)+.5*(T(NI,J-1)+T(NI,J+1))+BTA)/TPBI
        TNEW(NI,NJ)=(T(NI,LJ)+T(LI,NJ)+2.*BTA)/TQBI
        DO 110 I=2,LI
```

```
      110 TNEW(I,NJ)=(T(I,LJ)+.5*(T(I+1,NJ)+T(I-1,NJ))+BTA)/TPBI
          TNEW(1,NJ)=(T(1,LJ)+T(2,NJ)+2.*BTA)/TQBI
          DO 111 J=2,LJ
      111 TNEW(1,J)=(T(2,J)+.5*(T(1,J-1)+T(1,J+1))+BTA)/TPBI
          TNEW(1,1)=(T(1,2)+T(2,1)+2.*BTA)/TQBI
          DO 202 I=1,NI
          DO 202 J=1,NJ
VI        IF(ABS(T(I,J)-TNEW(I,J))-EPS) 202,202,203
      202 CONTINUE
          GO TO 210
      203 DO 204 I=1,NI
          DO 204 J=1,KJ
      204 T(I,J)=TNEW(I,J)
          DO 205 I=K3I,NI
          DO 205 J=MJ,MMJ
VII   205 T(I,J)=TNEW(I,J)
          DO 206 I=1,NI
          DO 206 J=K3J,NJ
      206 T(I,J)=TNEW(I,J)
          DO 207 I=1,KI
          DO 207 J=MJ,MMJ
      207 T(I,J)=TNEW(I,J)
          GO TO 200
      210 DO 211 I=1,NI
          ND=NI-I+1
VIII  211 WRITE(6,212) (TNEW(ND,J),J=1,NJ)
      212 FORMAT(1H0,///(10F10.7))
          STOP
          END
$DATA
 16 16  6  5  9  9  10.     0.       1.       .00001
```

APPENDIX E

COMPUTER PROGRAM TO PREDICT CAVITY GEOMETRY FOR THE SYSTEM GIVEN IN APPENDIX D

Table 6

Definitions of Input Variables for the Program Given in Appendix E

Variable Name	Definition
NI*	Number of nodal points in I-direction
NJ	Number of nodal points in J-direction
TT	$(T-T_A)/(T_B-T_A)$ evaluated at the lower boundary, i.e. $(T_B-T_A)/(T_B-T_A)=1$
TA	$(T_A-T_A)/(T_B-T_A)=0$ in this program
T(NI,J)	Bottom surface temperature data
T(I,NJ)	Right side surface temperature data (exclude 2 end points)
T(1,J)	Top surface temperature data
T(I,1)	Left side surface temperature data (exclude 2 end points)

*Refer to Figure 27 for nodal locations. Square meshes are used in this computer program.

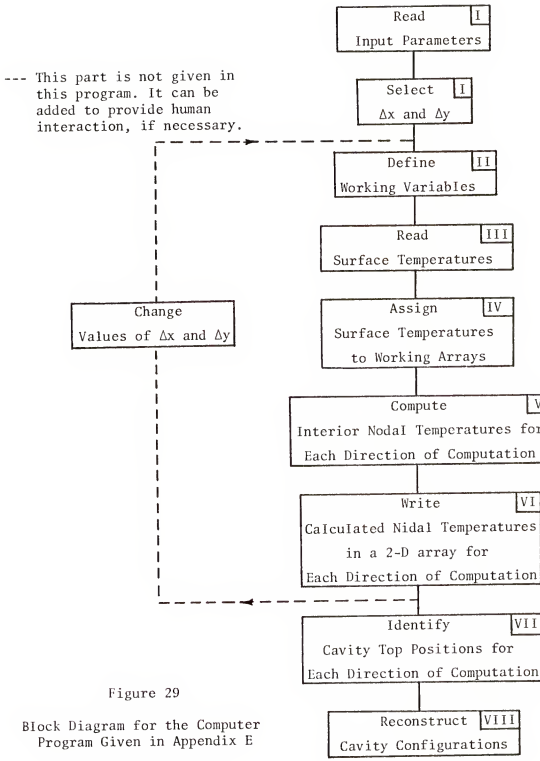

Figure 29

Block Diagram for the Computer Program Given in Appendix E

```
C
C       THIS PROGRAM PREDICTS THE POSSIBLE CAVITY CONTOUR
C       INSIDE OF A PARALLELPIPED BLOCK WITH GIVEN SURFACE
C       TEMPERATURE DISTRIBUTIONS. DATA SMOOTH ROUTINE
C       (1-6-1) APPLIED ON CALCULATED VALUES.
C
        INTEGER DOT,CROSS,A1,A2,A3,A4
        DIMENSION T(16,16),T1(16,16),T2(16,16),A1(16,16),
       /          A2(16,16),A3(16,16),A4(16,16),
       /          T3(16,16),T4(16,16)
I       DATA DOT,CROSS,BLANK,FILLED/0,1,1H ,1HM/
        READ (5,101) NI,NJ,BT,TA
  101   FORMAT (2I3,2F5.2)
        LI=NI-1
        LJ=NJ-1
        DL=LJ
II      DEL=1./DL
        BI=BT*DEL
        TPBI=2.+BI
        READ (5,102) (T(NI,J),J=1,NJ)
  102   FORMAT (8F10.7)
III     READ (5,102) (T(I,NJ),I=2,LI)
        READ (5,102) (T(1,J),J=1,NJ)
        READ (5,102) (T(I,1),I=2,LI)
        DO 105 J=1,NJ
        T2(NI,J)=T(NI,J)
        T3(NI,J)=T(NI,J)
        T4(NI,J)=T(NI,J)
  105   T1(NI,J)=T(NI,J)
        DO 106 I=2,LI
        T2(I,NJ)=T(I,NJ)
        T3(I,NJ)=T(I,NJ)
        T4(I,NJ)=T(I,NJ)
  106   T1(I,NJ)=T(I,NJ)
        DO 107 J=1,NJ
IV      T2(1,J)=T(1,J)
        T3(1,J)=T(1,J)
        T4(1,J)=T(1,J)
  107   T1(1,J)=T(1,J)
        DO 108 I=2,LI
        T2(I,1)=T(I,1)
        T3(I,1)=T(I,1)
        T4(I,1)=T(I,1)
  108   T1(I,1)=T(I,1)
        DO 120 J=2,LJ
  120   T(2,J)=T(1,J)*TPBI-(T(1,J-1)+T(1,J+1))/2.-TA*BI
        DO 121 J=2,LJ
  121   T1(2,J)=(T(2,J-1)+6.*T(2,J)+T(2,J+1))/8.
        DO 130 I=3,LI
        DO 131 J=2,LJ
  131   T(I,J)=4.*T(I-1,J)-T(I-1,J-1)-T(I-1,J+1)-T(I-2,J)
        DO 132 J=2,LJ
```

```
      T1(I,J)=(T(I,J-1)+6.*T(I,J)+T(I,J+1))/8.
  130 CONTINUE
      DO 140 J=2,LJ
  140 T(LI,J)=T(NI,J)*TPBI-(T(NI,J-1)+T(NI,J+1))/2.-TA*BI
      DO 141 J=2,LJ
  141 T2(LI,J)=(T(LI,J-1)+6.*T(LI,J)+T(LI,J+1))/8.
      DO 142 I=3,LI
      NA=NI-I+1
      DO 143 J=2,LJ
  143 T(NA,J)=4.*T(NA+1,J)-T(NA+1,J-1)-T(NA+1,J+1)-T(NA+2,J)
      DO 144 J=2,LJ
  144 T2(NA,J)=(T(NA,J-1)+6.*T(NA,J)+T(NA,J+1))/8.
  142 CONTINUE
      DO 160 I=2,LI
  160 T(I,2)=T(I,1)*TPBI-(T(I-1,1)+T(I+1,1))/2.-TA*BI
      DO 161 I=2,LI
  161 T3(I,2)=(T(I-1,2)+6.*T(I,2)+T(I+1,2))/8.
      DO 170 J=3,LJ
      DO 171 I=2,LI
  171 T(I,J)=4.*T(I,J-1)-T(I-1,J-1)-T(I+1,J-1)-T(I,J-2)
      DO 172 I=2,LI
  172 T3(I,J)=(T(I-1,J)+6.*T(I,J)+T(I+1,J))/8.
  170 CONTINUE
      DO 180 I=2,LI
  180 T(I,LJ)=T(I,NJ)*TPBI-(T(I-1,NJ)+T(I+1,NJ))/2.-TA*BI
      DO 181 I=2,LI
  181 T4(I,LJ)=(T(I-1,LJ)+6.*T(I,LJ)+T(I+1,LJ))/8.
      DO 182 J=3,LJ
      NB=NJ-J+1
      DO 183 I=2,LI
  183 T(I,NB)=4.*T(I,NB+1)-T(I-1,NB+1)-T(I+1,NB+1)-T(I,NB+2)
      DO 184 I=2,LI
  184 T4(I,NB)=(T(I-1,NB)+6.*T(I,NB)+T(I+1,NB))/8.
  182 CONTINUE
      WRITE (6,202)
      DO 200 I=1,NI
      NA=NI-I+1
  200 WRITE(6,201) (T1(NA,J),J=1,NJ)
  201 FORMAT (1H0,/16F7.4)
      WRITE (6,202)
  202 FORMAT (1H1)
      DO 203 I=1,NI
      NA=NI-I+1
  203 WRITE (6,201) (T2(NA,J),J=1,NJ)
      WRITE (6,202)
      DO 260 I=1,NI
      NA=NI-I+1
  260 WRITE (6,201) (T3(NA,J),J=1,NJ)
      WRITE (6,202)
      DO 280 I=1,NI
      NA=NI-I+1
  280 WRITE (6,201) (T4(NA,J),J=1,NJ)
```

```
      WRITE (6,202)
      DO 210 I=1,NI
      NA=NI-I+1
      DO 211 J=1,NJ
      IF (ABS(T1(NA,J))-0.99 ) 212,213,213
  212 A1(NA,J)=DOT
      GO TO 211
  213 A1(NA,J)=CROSS
  211 CONTINUE
  210 CONTINUE
      WRITE(6,310)
  310 FORMAT(////1X,24HAPPROACH FROM THE BOTTOM)
      DO 214 I=1,NI
      NA=NI-I+1
  214 WRITE (6,215) (A1(NA,J),J=1,NJ)
  215 FORMAT (1H0,/1X,16I4)
      WRITE (6,202)
      DO 220 I=1,NI
      NA=NI-I+1
      DO 221 J=1,NJ
      IF (ABS(T2(NA,J))-0.99) 222,223,223
  222 A2(NA,J)=DOT
      GO TO 221
  223 A2(NA,J)=CROSS
  221 CONTINUE
  220 CONTINUE
      WRITE(6,311)
  311 FORMAT(////1X,21HAPPROACH FROM THE TOP)
      DO 224 I=1,NI
      NA=NI-I+1
  224 WRITE (6,215) (A2(NA,J),J=1,NJ)
      WRITE (6,202)
      DO 290 I=1,NI
VII   NA=NI-I+1
      DO 291 J=1,NJ
      IF (ABS(T3(NA,J))-0.99) 292,293,293
  292 A3(NA,J)=DOT
      GO TO 291
  293 A3(NA,J)=CROSS
  291 CONTINUE
  290 CONTINUE
      WRITE(6,312)
  312 FORMAT(////1X,21HAPPROACH FROM THE LHS)
      DO 294 I=1,NI
      NA=NI-I+1
  294 WRITE (6,215) (A3(NA,J),J=1,NJ)
      WRITE (6,202)
      DO 300 I=1,NI
      NA=NI-I+1
      DO 301 J=1,NJ
      IF (ABS(T4(NA,J))-0.99) 302,303,303
  302 A4(NA,J)=DOT
```

```
      GO TO 301
  303 A4(NA,J)=CROSS
  301 CONTINUE
  300 CONTINUE
      WRITE(6,313)
  313 FORMAT(////1X,21HAPPROACH FROM THE RHS)
      DO 304 I=1,NI
      NA=NI-I+1
  304 WRITE (6,215) (A4(NA,J),J=1,NJ)
      DO 305 I=1,NI
      DO 305 J=1,NJ
      A1(I,J)=A1(I,J)+A2(I,J)+A3(I,J)+A4(I,J)
      IF (A1(I,J) .EQ. 4) GO TO 306
VIII  T(I,J)=FILLED
      GO TO 305
  306 T(I,J)=BLANK
  305 CONTINUE
      WRITE(6,202)
      DO 307 I=1,NI
      NA=NI-I+1
  307 WRITE(6,308) (T(I,J),J=1,NJ)
  308 FORMAT(//1X,16A4)
      STOP
      END
```

APPENDIX F

COMPUTER PROGRAM FOR COMPUTATION OF SURFACE TEMPERATURES ON A PLANE WALL HAVING A PRESCRIBED CAVITY GEOMETRY, THE LOWER BOUNDARY SUBJECTED TO A CONSTANT HEAT FLUX

Table 7

Definitions of Input Variables for the Program Given in Appendix F

Variable Name	Definition
NI*	Number of nodal points in I-direction
NJ	Number of nodal points in J-direction
MI	Location of cavity boundary in the I-direction
MJ	Location of cavity boundary in the J-direction
QLK	$=qL/(kT_A)$, dimensionless heat flux, where q is heat flux, L is system length, k is thermal conductivity and T_A is ambient temperature
HK	$=hL/k$, Biot number, where h is convective heat transfer coefficient

*Refer to Figure 24 for definition of nodal locations. Square meshes are used in this computer program.

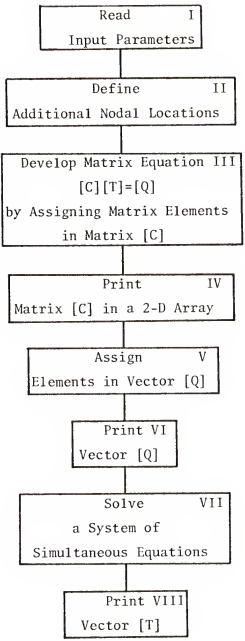

Figure 30

Block Diagram for the Computer Program Given in Appendix F

```
C
C       THIS PROGRAM EVALUATES THE SURFACE TEMPERATURE
C       NONUNIFORMITY AS A FUNCTION OF MATERIAL EROSION.
C       A TWO DIMENSIONAL MODEL IS BEING CONSIDERED.
C       THE EROSION IS MODELED USING A CAVITY OF RECTAN-
C       GULAR CROSS SECTION RECEIVING CONSTANT HEAT FLUX.
C       THE OUTER SURFACE IS A CONVECTIVE BOUNDARY. PLANES
C       OF SYMMETRY ARE USED TO REDUCE THE NUMBER OF NODES.
C       SUBROUTINE SIMQ FROM SSP IS APPLIED TO SOLVE THE
C       SYSTEM OF EQUATIONS.
C
      DIMENSION C(83,83),Q(83)
I     DATA NI,NJ,MI,MJ,QLK,HK/7,13,3,5,3.0,10./
      DL=NJ-1
      QXK=QLK/DL
      QYK=QLK/DL
      DEL=1./DL
      BI=HK*DEL
      TPBI=2.+BI
      NI1=NI-MI+1
II    MAJ=MJ-1
      MAP=MAJ-1
      NIP=NI1*MAP
      NIMAJ=NI1*MAJ
      KI=MI-1
      NIMJ=NIMAJ+NI
      NIMJ1=NIMJ+NI
      NIMJ2=NIMJ1+NI
      NIMJY=NIMAJ+NI*(NJ-MAJ)
      NIMJX=NIMJY-NI
      NIMJN=NIMJX-NI
C
C       *** TO FORM MATRIX C(I,J) ***
C
      DO 101 I=1,NIMJY
      DO 101 J=1,NIMJY
  101 C(I,J)=0.
      KI1=NI1-1
      KI3=NI1-2
      C(1,1)=2.
      C(1,NI1+1)=-1.
      DO 102 I=2,KI1
      C(I,NI1+I)=-2.
  102 C(I,I)=4.
      DO 103 I=1,KI1
      C(I,I+1)=-1.
  103 C(I+1,I)=-1.
      C(NI1,NI1)=TPBI
      NI2=2*NI1
      C(NI1,NI2)=-1.
      IMJ=MJ-2
      DO 104 I=1,IMJ
```

```
      I1=I+1
      I2=I+2
      INI=NI1*I
      INI1=NI1*I1
      INI2=NI1*I2
      C(INI+1,INI+2)=-2.
      C(INI1,INI)=-0.5
      C(INI1,INI1)=TPBI
      C(INI1,INI2)=-0.5
      I0=I-1
      INI0=NI1*I0
      DO 105 J=1,KI1
      J1=J+1
      J2=J+2
      C(INI+J1,INI+J)=-1.
      C(INI+J1,INI+J2)=-1.
      C(INI+J,INI0+J)=-1.
      C(INI+J,INI+J)=4.
      C(INI+J,INI1+J)=-1.
  105 CONTINUE
      C(INI1,INI1+1)=0.
  104 CONTINUE
      INI=NI1*IMJ
      INI1=NI1*MAJ
III   INI2=NIMAJ+MI-1
      DO 126 J=1,NI1
      C(INI+J,INI1+J)=0.
      C(INI+J,INI2+J)=-1.
  126 CONTINUE
      C(NIMAJ,NIMJ)=-0.5
      C(NIMAJ+1,NIMAJ+1)=2.
      C(NIMAJ+1,NIMAJ+2)=-1.
      C(NIMAJ+1,NIMJ+1)=-1.
      KI2=MI-1
      DO 106 J=2,KI2
      J1=J-1
      J2=J+1
      C(NIMAJ+J,NIMAJ+J1)=-1.
      C(NIMAJ+J,NIMAJ+J)=4.
      C(NIMAJ+J,NIMAJ+J2)=-1.
      C(NIMAJ+J,NIMJ+J)=-2.
  106 CONTINUE
      NMI=NIMAJ+MI
      C(NMI,NIMAJ-KI1)=-1.
      C(NMI,NIMAJ+KI)=-1.
      C(NMI,NMI)=6.
      LI=MI+1
      C(NMI,NIMJ+MI)=-2.
      C(NMI,NIMAJ+LI)=-2.
      DO 107 J=2,KI1
      J1=J-1
      J2=J+1
```

```
      MIJ1=MI+J1-1
      C(NMI+J1,NIP+J)=-1.
      C(NMI+J1,NIMAJ+MIJ1)=-1.
      C(NMI+J1,NMI+J1)=4.
      C(NMI+J1,NMI+J)=-1.
      MIJ=MI+J1
      C(NMI+J1,NIMJ+MIJ)=-1.
  107 CONTINUE
      C(NIMJ,NIMAJ)=-0.5
      C(NIMJ,NIMJ-1)=-1.
      C(NIMJ,NIMJ)=TPBI
      C(NIMJ,NIMJ1)=-0.5
      NJJ=NJ-MJ-1
      LI1=NI-1
      DO 110 I=1,NJJ
      I1=I+1
      INI=NIMJ+NI*(I-1)
      INI1=NIMJ+NI*I
      INI2=NIMJ+NI*I1
      C(INI+1,INI+2)=-2.
  III C(INI1,INI)=-0.5
      C(INI1,INI1)=TPBI
      C(INI1,INI2)=-0.5
      DO 111 J=1,LI1
      INI0=INI-NI
      J1=J+1
      J2=J+2
      C(INI+J,INI0+J)=-1.
      C(INI+J1,INI+J)=-1.
      C(INI+J,INI+J)=4.
      C(INI+J1,INI+J2)=-1.
      C(INI+J,INI1+J)=-1.
  111 CONTINUE
      C(INI1,INI1+1)=0.
  110 CONTINUE
      C(NIMJX+1,NIMJN+1)=-1.
      C(NIMJX+1,NIMJX+1)=2.
      C(NIMJX+1,NIMJX+2)=-1.
      DO 112 J=1,LI1
      J1=J+1
      J2=J+2
      C(NIMJX+J1,NIMJN+J1)=-2.
      C(NIMJX+J1,NIMJX+J)=-1.
      C(NIMJX+J1,NIMJX+J1)=4.
      IF (NIMJX+J2 .GT. NIMJY) GO TO 112
      C(NIMJX+J1,NIMJX+J2)=-1.
  112 CONTINUE
      C(NIMJY,NIMJX)=-1.
      C(NIMJY,NIMJY)=TPBI
      KN=NIMJY/21
      IM=0
      NP1=1
```

```
      N21=21
  200 IM=IM+1
      WRITE (6,300)
IV    N2=IM*N21
      DO 114 I=1,NIMJY
  114 WRITE (6,115) (I,(C(I,J),J=NP1,N2))
  115 FORMAT (2X,I3,21F6.2)
      NP1=N2+1
      IF (IM .EQ. KN) GO TO 201
      GO TO 200
  201 N2=NIMJY
      WRITE (6,300)
  300 FORMAT (1H1)
      DO 214 I=1,NIMJY
  214 WRITE (6,115) (I,(C(I,J),J=NP1,N2))
C
C       *** TO FORM MATRIX Q(I) ***
C
      DO 116 I=1,NIMJY
  116 Q(I)=0.
      Q(1)=QXK
      DO 117 I=1,IMJ
      NI1I=NI1*I
  117 Q(NI1I+1)=2.*QXK
      Q(NIMAJ+1)=QXK+QYK
 V    DO 118 I=2,MI
  118 Q(NIMAJ+I)=2.*QYK
      DO 119 I=1,NJJ
      INI=NIMJ+NI*(I-1)+1
  119 Q(INI)=2.*QXK
      Q(NIMJX+1)=QXK
      WRITE (6,300)
VI    WRITE (6,120) (Q(I),I=1,NIMJY)
  120 FORMAT (5X,F10.4)
      DO 123 I=1,NIMJY
      Q(I)=Q(I)/4.
      DO 123 J=1,NIMJY
VII   C(I,J)=C(I,J)/4.
  123 CONTINUE
      CALL SIMQ(C,Q,NIMJY,KS)
      WRITE (6,125)
  125 FORMAT (1H1)
      DO 121 I=1,NIMJY
VIII121 WRITE (6,122) I,Q(I)
  122 FORMAT (5X,I3,F10.5)
      STOP
      END
```

APPENDIX G

COMPUTER PROGRAM TO PREDICT CAVITY GEOMETRY FOR THE SYSTEM GIVEN IN APPENDIX F

Table 8

Definitions of Input Variables for the Program Given in Appendix G

Variable Name	Definition
QLK	$=qL/(kT_A)$, dimensionless heat flux, where q is heat flux, L is system length, k is thermal conductivity and T_A is ambient temperature
CI	$=hL/k$, Biot number, where h is convective coefficient
CMU	$=\ell/L$, system aspect ratio, where ℓ is system thickness
DL*	Number of intervals taken in the J-direction
N	Number of eigenvalues desired
IEND	Maximum number of iteration steps desired for the solution of eigenvalues
MW	Number of nodal points on top surface of Z_1, =5 in this program
EPS	Input value which specifies the upper bound of the error of resultant eigenvalue x
M	Number of surface temperature data points taken as input
T	Input surface temperatures
W	Assumed cavity width

*Square meshes are used in this computer program.

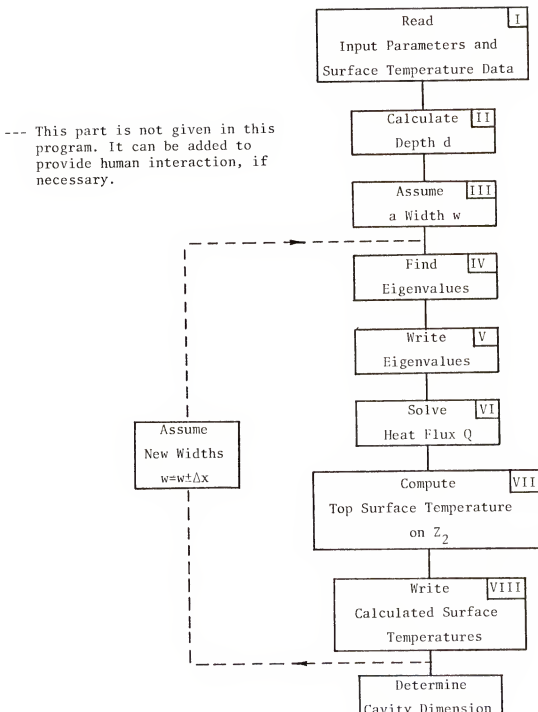

Figure 31

Block Diagram for the Computer Program Given in Appendix G

```
C
C       THIS PROGRAM PREDICTS POSSIBLE CAVITY DEPTH D AND
C       WIDTH W THROUGH SCANNED SURFACE TEMPERATURE DIS-
C       TRIBUTION T. THE LOWER BOUNDARY IS KNOWN TO BE
C       SUBJECTED TO A CONSTANT HEAT FLUX Q.
C       SUBROUTINES RTMI AND SIMQ FROM SSP ARE USED TO
C       SOLVE EIGENVALUES AND SIMULTANEOUS EQUATIONS
C       RESPECTIVELY.
C
        DIMENSION T(14), Q1(5), X1(20), X2(20),C(5,5),F(9)
        COMMON DMU,BI
        DATA QLK,CI,CMU,DL,N,IEND,MW,EPS/3.,10.,0.5,12.,20.,
     I  /                                    500,5,0.00001/
        EXTERNAL FCT1
        READ(5,103) M,(T(J),J=1,M)
      103 FORMAT(I3/(7F8.5))
        WRITE (6,202) (T(J),J=1,M)
C
C       **** PREDICT DEPTH D ****
C
        BI=CI
        QHT=QLK/BI
        DEL=1./DL
        IM=M-1
     II XIM=IM
        SUM=(T(1)+T(M))/2.-QHT
        DO 112 I=2,IM
      112 SUM=SUM+T(I)-QHT
        D=SUM/(QHT*XIM)
C
C       **** ASSUME A WIDTH W ****
C
        W=1./3.
        WRITE(6,114) D,W
    III 114 FORMAT(/5X,17HPREDICTED DEPTH= ,F7.4,
       /        /5X,17HASSUMED   WIDTH= ,F7.4)
        PI=3.141593
        VMD=CMU-D
        DO 101 I=1,N
        XI=I-1
        XL1=3.*XI*PI+0.01
        XR1=(3.*XI+1.5)*PI-0.01
        DMU=VMD
        CALL RTMI(X,FT,FCT1,XL1,XR1,EPS,IEND,IER)
     IV X1(I)=X
        XL1=2.*XI*PI+0.01
        XR1=(2.*XI+1.)*PI-0.01
        DMU=CMU
        CALL RTMI(XA,FT,FCT1,XL1,XR1,EPS,IEND,IER2)
        X2(I)=XA
        WRITE (6,102) X1(I),X2(I)
      V102 FORMAT (5X,2F10.6)
```

```
101 CONTINUE
    DBI=BI**2
    DEL1=DEL
    DO 107 I=1,MW
107 Q1(I)=T(I)-QHT
    DO 105 I=1,MW
    DO 105 J=1,MW
105 C(I,J)=0.
    DO 104 I=1,MW
    XI=I-1
    Z=XI*DEL1
    DO 106 IN=1,N
    XR=X1(IN)
    DX=XR**2
    DXB=DX+DBI
    A=XR*VMD
    A1=COS(A)
VI  B=XR*W
    B1=XR*SINH(B)
    VALUE=DEL*A1*2.*DXB/(3.*B1*(VMD*DXB+BI))*COSH(XR*Z)
    C(I,1)=C(I,1)+VALUE
    C(I,2)=C(I,2)+4.*VALUE*COS(XR*DEL)
    C(I,3)=C(I,3)+2.*VALUE*COS(2.*XR*DEL)
    C(I,4)=C(I,4)+4.*VALUE*COS(3.*XR*DEL)
    C(I,5)=C(I,5)+VALUE*COS(4.*XR*DEL)
106 CONTINUE
104 CONTINUE
    DO 111 I=1,MW
111 WRITE (6,203) (C(I,J),J=1,MW)
203 FORMAT(5X,5F8.5)
    CALL SIMQ(C,Q1,MW,KS)
    WRITE (6,201) (Q1(I),I=1,MW)
201 FORMAT(5X,F10.6)
    DO 110 I=1,9
110 F(I)=0.
    DO 108 I=2,9
    ZI=I+3
    Z=ZI*DEL
    ZD=1.-Z
    DO 109 IN=1,N
    XS=X2(IN)
    DXS=XS**2
    DBX=DBI+DXS
VII G1=QLK/XS*SIN(XS*D)
    F1=XS*(1.-W)
    G2=COSH(XS*ZD)
    F2=2.*DBX/(XS*SINH(F1)*(CMU*DBX+BI))*COS(XS*CMU)
    XD=XS*DEL
    G3=DEL/3.*(Q1(1)*COS(2.*XD)+4.*Q1(2)*COS(3.*XD)
   /          +2.*Q1(3)*COS(4.*XD)+4.*Q1(4)*COS(5.*XD)
   /          +Q1(5)*COS(6.*XD))
    F(I)=F(I)+F2*G2 *(G1-G3)
```

```
  109 CONTINUE
      F(I)=F(I)+GHT
  108 CONTINUE
      WRITE(6,202) (T(I),I=1,MW),(F(I),I=2,9)
VIII202 FORMAT(5X,13F8.5)
      STOP
      END
      FUNCTION FCT1(X)
      COMMON DMU,BI
      A=DMU*X
      FCT1=TAN(A)-BI/X
      RETURN
      END
$DATA
 13
 0.34529 0.34667 0.35048 0.35556 0.35974 0.36059 0.35817
 0.35382 0.34891 0.34444 0.34097 0.33880 0.33807
```

APPENDIX H

COMPUTER PROGRAM FOR COMPUTATION OF SURFACE TEMPERATURES FOR A RECTANGULAR PARALLELEPIPED WITH A PRESCRIBED RECTANGULAR HOLE IN IT, THE HOLE BOUNDARY SUBJECTED TO A CONSTANT HEAT FLUX

Table 9

Definitions of Input Variables for the Program Given in Appendix H

Variable Name	Definition
NI*	Number of nodal points in I-direction
NJ	Number of nodal points in J-direction
MI	Location of cavity bottom boundary
KI	Location of cavity top boundary
MJ	Location of cavity left boundary
KJ	Location of cavity right boundary
QLK	$=qL/(kT_A)$, dimensionless heat flux, where q is surface heat flux, L is system length (in J-direction), k is thermal conductivity and T_A is ambient temperature
HK	$=hL/k$, Biot number, where h is convective heat transfer coefficient

*Refer to Figure 27 for definition of nodal locations, note that the nodes MMI and MMJ are replaced by KI and KJ respectively in this program. Square meshes are used in this computer program.

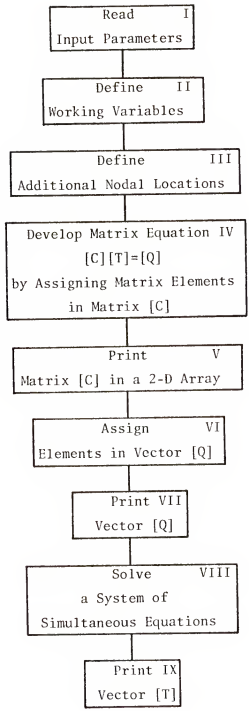

Figure 32

Block Diagram for the Computer Program Given in Appendix H

```
C
C       THIS PROGRAM EVALUATES THE SURFACE TEMPERATURE
C       DISTRIBUTION OF A RECTANGULAR PARALLELPIPED
C       WITH A PRESCRIBED RECTANGULAR HOLE IN IT. THE
C       HOLE BOUNDARY IS SUBJECTED TO A CONSTANT HEAT
C       FLUX Q. THE OUTSIDE SURFACE IS A CONVECTIVE
C       BOUNDARY. SUBROUTINE SIMQ FROM SSP IS USED TO
C       SOLVE THE SYSTEM OF SIMULTANEOUS EQUATIONS.
C
        DIMENSION C(161,161),Q(161)
    I   DATA NI,NJ,MI,MJ,KI,KJ,QLK,HK/13,13,8,4,11,9,
       /                                3.0,10./
        DL=NJ-1
        QXK=QLK/DL
        BI=HK/DL
   II   TPBI=2.+BI
        A=-0.5
        B=-1.0
        NINJ=NI*NJ-(KI-MI-1)*(KJ-MJ-1)
        MJ1=MJ-1
        MJ2=MJ-2
  III   MJ1NI=MJ1*NI
        MJ2NI=MJ2*NI
        NIMJ=NI*MJ
C
C         *** TO FORM MATRIX C(I,J) ***
C
        DO 101 I=1,NINJ
        DO 101 J=1,NINJ
  101   C(I,J)=0.
        C(1,1)=1.+BI
        DO 102 I=2,NI
        C(I,I)=TPBI
        C(I-1,I)=A
        C(I,I-1)=A
        C(I,NI+I)=B
  102   CONTINUE
        C(1,NI+1)=A
        C(NI,NI)=1.+BI
        C(NI,NI+NI)=A
        DO 103 J=1,MJ2
   IV   NIJ=NI*J
        NIJ1=NI*(J-1)
        NIJ2=NI*(J+1)
        DO 104 I=1,NI
        C(NIJ+I,NIJ+I)=2.0
        C(NIJ+I,NIJ1+I)=A
        C(NIJ+I,NIJ+I-1)=A
        C(NIJ+I,NIJ+I+1)=A
        C(NIJ+I,NIJ2+I)=A
  104   CONTINUE
        C(NIJ+1,NIJ+1)=TPBI
```

```
      C(NIJ+1,NIJ)=0.
      C(NIJ+1,NIJ+2)=B
      C(NIJ2,NIJ2-1)=B
      C(NIJ2,NIJ2)=TPBI
      C(NIJ2,NIJ2+1)=0.
  103 CONTINUE
      DO 105 I=1,MI
      IN=MJ1NI+I
      C(IN,IN)=2.
      C(IN,MJ2NI+I)=A
      C(IN,IN-1)=A
      C(IN,IN+1)=A
      C(IN,NIMJ+I)=A
  105 CONTINUE
      C(MJ1NI+1,MJ1NI+1)=TPBI
      C(MJ1NI+1,MJ1NI)=0.
      C(MJ1NI+1,MJ1NI+2)=B
      M1NM=MJ1NI+MI
      C(M1NM,M1NM)=3.
      C(M1NM,M1NM-1)=B
      C(M1NM,MJ2NI+MI)=B
      KMI1=KI-MI-1
IV    M2NM=MJ2NI+MI
      DO 106 I=1,KMI1
      C(M1NM+I,M1NM+I)=2.0
      C(M1NM+I,M1NM+I-1)=A
      C(M1NM+I,M1NM+I+1)=A
      C(M1NM+I,M2NM+I)=B
  106 CONTINUE
      M1NK=MJ1NI+KI
      C(M1NK,M1NK)=3.0
      C(M1NK,M1NK-1)=A
      C(M1NK,M1NK+1)=B
      C(M1NK,MJ2NI+KI)=B
      C(M1NK,NIMJ+MI+1)=A
      M2NK=MJ2NI+KI
      NIMM=NIMJ+MI
      NK=NI-KI
      DO 107 I=1,NK
      C(M1NK+I,M1NK+I)=2.0
      C(M1NK+I,M1NK+I-1)=A
      C(M1NK+I,M1NK+I+1)=A
      C(M1NK+I,M2NK+I)=A
      C(M1NK+I,NIMM+I+1)=A
  107 CONTINUE
      C(NIMJ,NIMJ)=TPBI
      C(NIMJ,NIMJ-1)=B
      C(NIMJ,NIMJ+1)=0.
      KMJ=KJ-MJ-1
      NKMI=NI-KI+MI+1
      NK1=NI-KI+1
      DO 108 J=1,KMJ
```

```
      JNKMI=(J-1)*NKMI
      JNIMJ=NIMJ+JNKMI
      DO 109 I=1,NKMI
      C(JNIMJ+I,JNIMJ+I)=2.
      IN=JNIMJ+I
      C(IN,IN-1)=A
      C(IN,IN+1)=A
      C(IN,IN+NKMI)=A
      C(IN,IN-NKMI)=A
  109 CONTINUE
      C(JNIMJ+1,JNIMJ+1)=TPBI
      C(JNIMJ+NKMI,JNIMJ+NKMI)=TPBI
      C(JNIMJ+1,JNIMJ)=0.
      C(JNIMJ+1,JNIMJ+2)=B
      C(JNIMJ+NKMI,JNIMJ+NKMI-1)=B
      C(JNIMJ+NKMI,JNIMJ+NKMI+1)=0.
      C(JNIMJ+MI,JNIMJ+MI-1)=B
      C(JNIMJ+MI,JNIMJ+MI+1)=0.
      C(JNIMJ+MI+1,JNIMJ+MI)=0.
      C(JNIMJ+MI+1,JNIMJ+MI+2)=B
  108 CONTINUE
      DO 130 I=1,MI
      IN=NIMJ+I
      C(IN,IN-NKMI)=0.
  130 C(IN,IN-NI)=A
      NIKN=NIMJ+KMJ*NKMI
      NIKN1=NIKN-NKMI
IV    NIKNM=NIKN+MI
      NIKN1M=NIKN1+MI
      DO 110 I=1,NK1
      C(NIMM+I,M1NM+I)=0.
      C(NIMM+I,M1NK+I-1)=A
      C(NIKN1M+I,NIKNM+I)=0.
      C(NIKN1M+I,NIKN+KI+I-1)=A
  110 CONTINUE
      NKNI=NIKN+NI
      DO 111 I=1,MI
      C(NIKN+I,NIKN+I)=2.
      C(NIKN+I,NIKN1+I)=A
      C(NIKN+I,NIKN+I-1)=A
      C(NIKN+I,NIKN+I+1)=A
      C(NIKN+I,NKNI+I)=A
  111 CONTINUE
      C(NIKN+1,NIKN+1)=TPBI
      C(NIKN+1,NIKN)=0.
      C(NIKN+1,NIKN+2)=B
      NKM=NIKN+MI
      NKNM=NKNI+MI
      C(NKM,NKM)=3.
      C(NKM,NKM-1)=B
      C(NKM,NKNM)=B
      DO 112 I=1,KMI1
```

```
      C(NKM+I,NKM+I)=2.
      C(NKM+I,NKM+I-1)=A
      C(NKM+I,NKM+I+1)=A
      C(NKM+I,NKNM+I)=B
  112 CONTINUE
      NKK=NIKN+KI
      C(NKK,NKK)=3.
      C(NKK,NKK-1)=A
      C(NKK,NKK+1)=B
      C(NKK,NKNI+KI)=B
      C(NKK,NIKN1+MI+1)=A
      DO 113 I=1,NK
      C(NKK+I,NKK+I)=2.
      C(NKK+I,NKK+I-1)=A
      C(NKK+I,NKK+I+1)=A
      C(NKK+I,NIKN1M+I+1)=A
      C(NKK+I,NKNI+KI+I)=A
  113 CONTINUE
      C(NKNI,NKNI)=TPBI
      C(NKNI,NKNI-1)=B
      C(NKNI,NKNI+1)=0.
      NKJ1=NJ-KJ-1
      DO 114 J=1,NKJ1
      NKJN=NKNI+(J-1)*NI
      NKJN1=NKNI+NI*J
      NIJN=NIKN+(J-1)*NI
IV    DO 115 I=1,NI
      IN=NKJN+I
      C(IN,IN)=2.
      C(IN,NIJN+I)=A
      C(IN,IN-1)=A
      C(IN,IN+1)=A
      C(IN,NKJN1+I)=A
  115 CONTINUE
      C(NKJN+1,NKJN+1)=TPBI
      C(NKJN+1,NKJN)=0.
      C(NKJN+1,NKJN+2)=B
      C(NKJN1,NKJN1)=TPBI
      C(NKJN1,NKJN1-1)=B
      C(NKJN1,NKJN1+1)=0.
  114 CONTINUE
      NINJ1=NINJ-NI
      NINJ2=NINJ1-NI
      C(NINJ1+1,NINJ1+1)=1.+BI
      DO 116 I=2,NI
      IN1=NINJ1+I
      C(IN1,IN1)=TPBI
      C(IN1-1,IN1)=A
      C(IN1,IN1-1)=A
      C(IN1,NINJ2+I)=B
  116 CONTINUE
      C(NINJ1+1,NINJ2+1)=A
```

```
      C(NINJ,NINJ)=1.+BI
      C(NINJ,NINJ1)=A
      KN=NINJ/21
      IM=0
      NP1=1
      N21=21
  200 IM=IM+1
      WRITE(6,300)
      N2=IM*N21
  V   DO 118 I=1,NINJ
  118 WRITE(6,119) (I,(C(I,J),J=NP1,N2))
  119 FORMAT(2X,I3,21F6.2)
      NP1=N2+1
      IF(IM .EQ. KN) GO TO 201
      GO TO 200
  201 N2=NINJ
      WRITE(6,300)
  300 FORMAT(1H1)
      DO 120 I=1,NINJ
  120 WRITE(6,119) (I,(C(I,J),J=NP1,N2))
C
C       *** TO FORM MATRIX Q(I) ***
C
      DO 121 I=1,NINJ
  121 Q(I)=0.
      KM1=KI-MI+1
      DO 122 I=1,KM1
  VI  I1=I-1
      Q(M1NM+I1)=QXK
  122 Q(NKM+I1)=QXK
      DO 123 J=1,KMJ
      NIM=NIMJ+(J-1)*NKMI+MI
      Q(NIM)=QXK
      Q(NIM+1)=QXK
  123 CONTINUE
      WRITE(6,300)
      DO 124 I=1,NINJ
 VII  124 WRITE(6,125) I,Q(I)
  125 FORMAT(2X,I3,F10.4)
      DO 126 I=1,NINJ
      Q(I)=Q(I)/2.
VIII  DO 126 J=1,NINJ
      C(I,J)=C(I,J)/2.
  126 CONTINUE
      CALL SIMQ(C,Q,NINJ,KS)
      WRITE(6,300)
      DO 127 I=1,NINJ
  IX  127 WRITE(6,125) I,Q(I)
      STOP
      END
```

APPENDIX I

COMPUTER PROGRAM FOR COMPUTATION OF SURFACE TEMPERATURES ON A PLANE WALL HAVING A PRESCRIBED CAVITY GEOMETRY, THE LOWER BOUNDARY SUBJECTED TO A CONVECTIVE CONDITION

Table 10

Definitions of Input Variables for the Program Given in Appendix I

Variable Name	Definition
NI*	Number of nodal points in I-direction
NJ	Number of nodal points in J-direction
MI	Location of cavity boundary in the I-direction
MJ	Location of cavity boundary in the J-direction
TH	Hot air temperature at the lower boundary [^{o}F]
TA	Ambient temperature [^{o}F]
VK	Thermal conductivity [Btu/hr ft ^{o}F]
EPS	Convergence criterion for iteration [^{o}F]
RE	Reynolds number of air flow at the lower boundary

*Refer to Figure 24 for definition of nodal locations. Square meshes are used in this computer program.

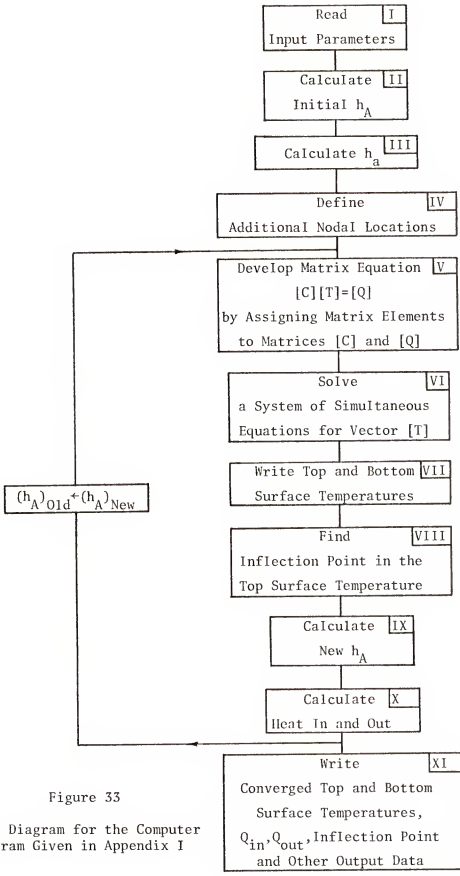

Figure 33

Block Diagram for the Computer Program Given in Appendix I

```
C      THIS PROGRAM EVALUATES THE SURFACE TEMPERATURE
C      NONUNIFORMITY AS A FUNCTION OF MATERIAL EROSION.
C      A TWO DIMENSIONAL MODEL IS BEING CONSIDERED.
C      THE EROSION IS MODELED USING A CAVITY OF RECTAN-
C      GULAR CROSS SECTION SUBJECTED TO HEAT CONVECTION.
C      THE OUTER SURFACE IS A CONVECTIVE BOUNDARY. PLANES
C      OF SYMMETRY ARE USED TO REDUCE THE NUMBER OF NODES.
C      A DIRECT METHOD (GAUSS ELLIMINATION) IS APPLIED TO
C      SOLVE THE SYSTEM OF EQUATIONS.
C
       DIMENSION C(151,151),Q(151),TBH(25),TT(25),TBV(25)
      /          ,TOLD(151),A(25)
   I   DATA NI,NJ,MI,MJ,TH,TA,VK,EPS,RE/7,25,5,7,200,.77,.
      /                                     1,.0,001,8000./
       DL=NJ-1
       DEL=1./DL
  II   DLT=(TH+TA)/2.
       KQ=0
       HH1=0.27*DLT**0.25
       HHB1=0.205*RE**0.731
       HVB1=HHB1
 III   HHB=HHB1*DEL/VK
       HVB=HVB1*DEL/VK
  180  BI=HH1*DEL/VK
       TPBI=2.+BI
       NI1=NI-MI+1
       MAJ=MJ-1
       MAP=MAJ-1
       NIP=NI1*MAP
  IV   NIMAJ=NI1*MAJ
       KI=MI-1
       NIMJ=NIMAJ+NI
       NIMJ1=NIMJ+NI
       NIMJ2=NIMJ1+NI
       NIMJY=NIMAJ+NI*(NJ-MAJ)
       NIMJX=NIMJY-NI
       NIMJN=NIMJX-NI
       DO 101 I=1,NIMJY
       DO 101 J=1,NIMJY
  101  C(I,J)=0.
       KI1=NI1-1
       KI3=NI1-2
   V   C(1,1)=2.+HHB
       C(1,NI1+1)=-1.
       DO 102 I=2,KI1
       C(I,NI1+I)=-2.
  102  C(I,I)=4.
       DO 103 I=1,KI1
       C(I,I+1)=-1.
  103  C(I+1,I)=-1.
       C(NI1,NI1)=TPBI
       NI2=2*NI1
```

```
      C(NI1,NI2)=-1.
      IMJ=MJ-2
      DO 104 I=1,IMJ
      I1=I+1
      I2=I+2
      INI=NI1*I
      INI1=NI1*I1
      INI2=NI1*I2
      C(INI+1,INI+2)=-2.
      C(INI1,INI)=-0.5
      C(INI1,INI1)=TPBI
      C(INI1,INI2)=-0.5
      I0=I-1
      INI0=NI1*I0
      DO 105 J=1,KI1
      J1=J+1
      J2=J+2
      C(INI+J1,INI+J)=-1.
      C(INI+J1,INI+J2)=-1.
      C(INI+J,INI0+J)=-1.
      C(INI+J,INI+J)=4.
      C(INI+J,INI1+J)=-1.
  105 CONTINUE
      C(INI1,INI1+1)=0.
      C(INI+1,INI+1)=4.+2.*HHB
  104 CONTINUE
      INI=NI1*IMJ
V     INI1=NI1*MAJ
      INI2=NIMAJ+MI-1
      DO 126 J=1,NI1
      C(INI+J,INI1+J)=0.
      C(INI+J,INI2+J)=-1.
  126 CONTINUE
      C(NIMAJ,NIMJ)=-0.5
      C(NIMAJ+1,NIMAJ+1)=2.+HHB+HVB
      C(NIMAJ+1,NIMAJ+2)=-1.
      C(NIMAJ+1,NIMJ+1)=-1.
      KI2=MI-1
      DO 106 J=2,KI2
      J1=J-1
      J2=J+1
      C(NIMAJ+J,NIMAJ+J1)=-1.
      C(NIMAJ+J,NIMAJ+J)=4.+2.*HVB
      C(NIMAJ+J,NIMAJ+J2)=-1.
      C(NIMAJ+J,NIMJ+J)=-2.
  106 CONTINUE
      NMI=NIMAJ+MI
      C(NMI,NIMAJ-KI1)=-1.
      C(NMI,NIMAJ+KI)=-1.
      C(NMI,NMI)=6.+HVB+HHB
      LI=MI+1
      C(NMI,NIMJ+MI)=-2.
```

```
      C(NMI,NIMAJ+LI)=-2.
      DO 107 J=2,KI1
      J1=J-1
      J2=J+1
      MIJ1=MI+J1-1
      C(NMI+J1,NIP+J)=-1.
      C(NMI+J1,NIMAJ+MIJ1)=-1.
      C(NMI+J1,NMI+J1)=4.
      C(NMI+J1,NMI+J)=-1.
      MIJ=MI+J1
      C(NMI+J1,NIMJ+MIJ)=-1.
  107 CONTINUE
      C(NIMJ,NIMAJ)=-0.5
      C(NIMJ,NIMJ-1)=-1.
      C(NIMJ,NIMJ)=TPBI
      C(NIMJ,NIMJ1)=-0.5
      NJJ=NJ-MJ-1
      LI1=NI-1
      DO 110 I=1,NJJ
      I1=I+1
      INI=NIMJ+NI*(I-1)
      INI1=NIMJ+NI*I
      INI2=NIMJ+NI*I1
      C(INI+1,INI+2)=-2.
V     C(INI1,INI)=-0.5
      C(INI1,INI1)=TPBI
      C(INI1,INI2)=-0.5
      DO 111 J=1,LI1
      INI0=INI-NI
      J1=J+1
      J2=J+2
      C(INI+J,INI0+J)=-1.
      C(INI+J1,INI+J)=-1.
      C(INI+J,INI+J)=4.
      C(INI+J1,INI+J2)=-1.
      C(INI+J,INI1+J)=-1.
  111 CONTINUE
      C(INI1,INI1+1)=0.
      C(INI+1,INI+1)=4.+2.*HHB
  110 CONTINUE
      C(NIMJX+1,NIMJN+1)=-1.
      C(NIMJX+1,NIMJX+1)=2.+HHB
      C(NIMJX+1,NIMJX+2)=-1.
      DO 112 J=1,LI1
      J1=J+1
      J2=J+2
      C(NIMJX+J1,NIMJN+J1)=-2.
      C(NIMJX+J1,NIMJX+J)=-1.
      C(NIMJX+J1,NIMJX+J1)=4.
      IF (NIMJX+J2 .GT. NIMJY) GO TO 112
      C(NIMJX+J1,NIMJX+J2)=-1.
  112 CONTINUE
```

```
      C(NIMJY,NIMJX)=-1.
      C(NIMJY,NIMJY)=TPBI
      DO 116 I=1,NIMJY
  116 Q(I)=0.
      BTA=BI*TA
      QXK=HHB*TH
      QYK=HVB*TH
      Q(NI1)=BTA
      Q(1)=QXK
      DO 117 I=1,IMJ
V     NI1I=NI1*I
      Q(NI1I+NI1)=BTA
  117 Q(NI1I+1)=2.*QXK
      Q(NIMAJ+1)=QXK+QYK
      Q(NIMAJ+NI)=BTA
      DO 118 I=2,KI
  118 Q(NIMAJ+I)=2.*QYK
      Q(NIMAJ+MI)=QXK+QYK
      DO 119 I=1,NJJ
      INI=NIMJ+NI*(I-1)
      Q(INI+NI)=BTA
  119 Q(INI+1)=2.*QXK
      Q(NIMJX+1)=QXK
      Q(NIMJY)=BTA
      DO 123 I=1,NIMJY
      Q(I)=Q(I)/4.
VI    DO 123 J=1,NIMJY
      C(I,J)=C(I,J)/4.
  123 CONTINUE
      CALL SIMQ(C,Q,NIMJY,KS)
      TBH(1)=Q(1)
      TT(1)=Q(NI1)
      DO 150 I=2,MAJ
      INI1=NI1*I
      I1=I-1
      INI=NI1*I1
      TT(I)=Q(INI1)
  150 TBH(I)=Q(INI+1)
      DO 151 I=1,MI
      J=MI-I+1
  151 TBV(I)=Q(NIMAJ+J)
      KNJ=NJ-1
      J=0
VII   DO 152 I=MJ,KNJ
      INI=NIMJ+J*NI
      TT(I)=Q(INI)
      TBH(I)=Q(INI+1)
  152 J=J+1
      TT(NJ)=Q(NIMJY)
      WRITE(6,153) (TT(I),I=1,NJ)
  153 FORMAT(1H1,(2X,13F10.5))
      WRITE(6,154) (TBH(I),I=1,MAJ)
```

```
  154 FORMAT(//////2X,4F10.5)
      DO 155 I=1,MI
  155 WRITE(6,156) TBV(I)
  156 FORMAT(42X,F10.5)
      WRITE(6,157) (TBH(I),I=MJ,KNJ)
  157 FORMAT(52X,8F10.5)
      NA=NJ-1
      DO 30 J=1,NA
   30 A(J)=TT(J)-TT(J+1)
VIII  CALL MAXSLP(A,NA,TFL,IP)
      POS=IP
      PINFL=(POS-0.5)*DEL
      XNJ=NJ
      XKNJ=KNJ
      XMI=MI
      TTM=0.
      TBHM=0.
      TBVM=0.
      DO 158 I=1,NJ
  158 TTM=TTM+TT(I)
   IX 
      TTM=TTM/XNJ
      DO 159 I=1,MI
  159 TBVM=TBVM+TBH(I)
      TBVM=TBVM/XMI
      DO 160 I=1,KNJ
  160 TBHM=TBHM+TBH(I)
      TBHM=TBHM/XKNJ
      HH=0.27*(TTM-TA)**0.25
      SUM1=0.
      SUM2=0.
      SUM3=0.
      SUM4=0.
      DO 161 I=2,KNJ
  161 SUM1=SUM1+HH1*(TT(I)-TA)
      QOUT=(SUM1+HH1*(TT(1)+TT(NJ)-2.*TA)*0.5)*DEL
      DO 162 I=2,MAJ
  162 SUM2=SUM2+HHB1*(TH-TBH(I))
      SUM2=SUM2+HHB1*(TH-TBH(1))*0.5
      DO 163 I=2,KI2
  163 SUM3=SUM3+HVB1*(TH-TBV(I))
      SUM3=SUM3+0.5*HVB1*(2.*TH-TBV(1)-TBV(MI))
      SUM3=SUM3+0.5*HHB1*(2.*TH-TBV(1)-TBV(MI))
    X 
      LNJ=KNJ-1
      DO 164 I=MJ,LNJ
  164 SUM4=SUM4+HHB1*(TH-TBH(I))
      SUM4=SUM4+HHB1*(TH-TBH(KNJ))*0.5
      QIN=(SUM2+SUM3+SUM4)*DEL
      WRITE(6,165) QIN,QOUT,HH,HHB1,HVB1,PINFL
  165 FORMAT(1H0,2X,6F10.5)
      KQ=KQ+1
      IF(KQ .EQ. 1) GO TO 169
      DO 168 I=1,NIMJY
```

```
      IF(ABS(Q(I)-TOLD(I))-EPS) 168,168,169
  168 CONTINUE
XI    GO TO 170
  169 DO 166 I=1,NIMJY
  166 TOLD(I)=Q(I)
      HH1=HH
      GO TO 180
  170 PUNCH 171, NI,NJ,MI,MJ,TH,TA,VK
  171 FORMAT(4I3,3F7.2)
XII   PUNCH 173, (TT(I),I=1,NJ)
  173 FORMAT (8F10.5)
      END
      SUBROUTINE MAXSLP(B,N,VAL,IO)
      DIMENSION B(13)
      VAL=0.
      IO=0
      DO 1 I=1,N
      IF (B(I) .LE. VAL) GO TO 1
      VAL=B(I)
      IO=I
    1 CONTINUE
      RETURN
      END
```

REFERENCES

1. Stolz, G., Jr., "Numerical Solutions to an Inverse Problem of Heat Conduction for Simple Shapes," Journal of Heat Transfer, TRANS. ASME, Volume 82, Series C, 1960, pp. 20-26.

2. Frank, I., "An Application of Least Squares Method to the Solution of the Inverse Problem of Heat Conduction," Journal of Heat Transfer, TRANS. ASME, Volume 85, Series C, pp. 378.

3. Burggraf, O.R., "An Exact Solution of the Inverse Problem in Heat Conduction Theory and Applications," Journal of Heat Transfer, Volume 86, Series C, 1964, pp. 373-382.

4. Sparrow, E.M., Haji-Sjeikh, A., and Lundgren, T.S., "The Inverse Problem in Transient Heat Conduction," Journal of Applied Mechanics, TRANS. AMSE, Volume 86, Series E, 1964, pp. 369-375.

5. Beck, J.V., Discussion to "The Inverse Problem in Transient Heat Conduction," Journal of Applied Mechanics, TRANS. ASME, Volume 87, Series E, 1965, pp. 472-473.

6. Beck, J.V., and Wolf, H., "The Nonlinear Inverse Heat Conduction Problem," ASME Paper No. 65-HT 40, 1965.

7. Beck, J.V., "Nonlinear Estimation Applied to the Nonlinear Inverse Heat Conduction Problem," International Journal of Heat and Mass Transfer, Volume 13, 1970, pp. 703-716.

8. Hsieh, C.K., and Ellingson, W.A., "The Feasibility of Using Infrared Scanning to Test Flaws in Ceramic Materials," Proceedings of the Fifteenth International Thermal Conductivity Conference, Plenum Press, New York, 1978, pp. 11-22.

9. Hsieh, C.K., Ellingson, W.A., and Su, K.C., "A Model Study for Quantitative Flaw Detection Using Infrared Scanning," British Journal of Nondestructive Testing, in press.

10. Hsieh, C.K., Ellingson, W.A., and Su, K.C., "Computer Modeling of Heat Transfer Through Refractory Lined Transfer Lines in Coal Gasification System," Argonne National Laboratory Technical Report, in press.

11. Kutzscher, E.W., and Zimmermann, K.H., "A Scanning Infrared Inspection System Applied to Nondestructive Testing of Bonded Aerospace Structures," Applied Optics, Volume 7, Number 9, 1968, pp. 1715-1720.

12. Dixon, R.D., Lassahn, G.D., and DiGiallonard, A., "Infrared Thermography of Subsurface Defects," Materials Evaluation, Volume 30, Number 4, 1972, pp. 73-80.

13. McCullough, L.D., and Green, D.R., "Electrothermal Nondestructive Testing of Metal Structures," Materials Evaluation, Volume 30, Number 4, 1972, pp. 87-93.

14. Barnes, R.B., "Diagnostic Thermography," Applied Optics, Volume 7, Number 9, 1968, pp. 1673-1685.

15. Ryan, J., "Thermography," Australian Radiology, Volume 13, Number 1, 1969, pp. 23.

16. Herma van Voss, S.F.C., and Thomas, P., Medical Thermography, S. Karger Publisher, Switzerland, 1969.

17. Haberman, J.D., "Image Analysis of Medical Infrared Thermograms," CRC Critical Reviews in Radiological Sciences, Chemical Rubber Company, Cleveland, 1971, pp. 427-465.

18. Chen, M.M., Pederson, C.O., and Chato, J.C., "On the Feasibility of Obtaining Three-Dimensional Information from Thermographic Measurements," Journal of Biomedical Engineering, TRANS. ASME, Volume 99, Series K, Number 2, 1977, pp. 58-64.

19. Gambarelli, J., Guerinel, G., Chevrot, L., and Mattei, M., Computerized Axial Tomography, Springer-Verlag, Berlin Heidelberg, 1978.

20. Tou, J.T., and Gonzalez, R.C., Pattern Recognition Principles, Addision-Wesley, Reading, Mass., 1974, p. 17.

21. Hsieh, C.K., Yang, M.C.K., Farber, E.A., and Jorolan, A., "A Feasibility Study to Test Structure Integrity by Infrared Scanning Technique," Thermal Conductivity, Proceedings of the Fourteenth International Conference on Thermal Conductivity, Plenum Press, New York, 1975, pp. 521-530.

22. Yang, M.C.K., and Hsieh, C.K., "A Three Component Method of Data Analysis for Nondestructive Testing by Infrared Scanning," Proceedings of the Society of Photo-Optical Instrumentation Engineers, Volume 95, 1976, pp. 212-216.

23. Private communication with TPRC, Purdue University.

24. Clausing, A.M., "Numerical Methods in Heat Transfer," Advanced Heat Transfer (Editor: B.T. Chao), University of Illinois Press, Urbana, 1969, p. 188.

25. Holman, J.P., Heat Transfer, Fourth Edition, McGraw-Hill, New York, 1976.

26. Gebhart, B., Heat Transfer, Second Edition, McGraw-Hill, New York 1971, p. 274.

27. Hsieh, C.K., and Su, K.C., "Design, Construction and Analysis of Continuous-Temperature Infrared Calibrator for Temperature Measurement Using an Infrared Scanner," to appear in July 1979 issue of the Review of Scientific Instruments.

28. Balcerzak, M.J., and Raynor, S., "Steady State Temperature Distribution and Heat Flow in Prismatic Bars with Isothermal Boundary Conditions," International Journal Heat and Mass Transfer, Volume 3, 1061, pp. 113-125.

29. Carslaw, H.S., and Jaeger, J.C., Conduction of Heat in Solids, Second Edition, Oxford, 1959, pp. 441-454.

30. Sholokhov, A.A., Inzh, Fiz. Zh. (in Russian), Volume 6, 1963, pp. 76.

31. Laura, P., and Chi, M., "Approximate Method for the Study of Heat Conduction in Bars of Arbitrary Cross Section," Journal of Heat Transfer, Trans. ASME, Volume C86, 1964, pp. 466-467.

32. Kumar, I.J., "Recent Mathematical Methods in Heat Transfer," Advances in Heat Transfer (Hartnett, J.P. and Irvine, T.F., Jr., Editors), Volume 8, Academic Press, New York, 1972, pp. 56.

33. Kantorovich, L.V. and Krylov, V.I., Approximate Methods of Higher Analysis, Interscience, New York, 1958, pp. 616-670.

34. Siegel, R., "Conformal Mapping for Steady Two-Dimensional Solidification on a Cold Surface in Flowing Liquid," NASA TN D-4771, 1968.

35. Hsieh, C.K., and Ellingson, W.A., "A Quantitative Determination of Surface Temperatures Using an Infrared Camera," SPIE Proceedings, Volume 124, 1977, pp. 228-235.

36. Scheffler, W.A., "Heat Conduction in Bodies with Small Boundary Perturbations," Journal of Heat Transfer, Trans. ASME, Volume 96C, 1974, pp. 248-249.

BIOGRAPHICAL SKETCH

Kuo Chin Su, was born December 3, 1949, in Paiho, Taiwan, China. He received his early childhood education in his hometown, and high school education in Chiyi, a city 10 miles away from home. After graduating from high school, he entered National Taiwan University (NTU) in Taipei, Taiwan, where he earned a Bachelor of Science degree in Mechanical Engineering. While matriculating at NTU, he tutored mathematics and physics to support his expenses for practicing photography. He also was a member of the Rocket Research Club and the Karate Association. After graduating from college, he served two years as a second lieutenant in the R.O.C. Army. On July 24, 1974, he married Jew Whei Lai, a girl he had known for ten years, and now they have a lovely daughter called Ying Ting. After his marriage he attended the University of Florida to pursue graduate study. He received his Master of Science degree in aerospace engineering in August, 1975, from the Engineering Sciences Department and has been pursuing a Doctor of Philosophy degree in mechanical engineering since December of 1976. He is a student member of the American Society of Mechanical Engineers (ASME) and the American Society of Heating, Refrigerating and Air Conditioning Engineers (ASHRAE). Honorary memberships include Tau Beta Pi and Pi Tau Sigma.

I certify that I have read this study and that in my opinion it conforms to acceptable standards of scholarly presentation and is fully adequate, in scope and quality, as a dissertation for the degree of Doctor of Philosophy.

C. K. Hsieh

C.K. Hsieh, Chairman
Associate Professor of Mechanical Engineering

I certify that I have read this study and that in my opinion it conforms to acceptable standards of scholarly presentation and is fully adequate, in scope and quality, as a disseration for the degree of Doctor of Philosophy.

R.K. Irey
Professor of Mechanical Engineering

I certify that I have read this study and that in my opinion it conforms to acceptable standards of scholarly presentation and is fully adequate, in scope and quality, as a dissertation for the degree of Doctor of Philosophy.

R A Gater

R.A. Gater
Associate Professor of Mechanical Engineering

I certify that I have read this study and that in my opinion if conforms to acceptable standards of scholarly presentation and is fully adequate, in scope and quality, as a disseratation for the degree of Doctor of Philosophy.

H.A. Ingley, III
Assistant Professor of Mechanical Engineering

I certify that I have read this study and that in my opinion it conforms to acceptable standards of scholarly presentation and is fully adequate, in scope and quality, as a dissertation for the degree of Doctor of Philosophy.

C. Luehr

C. Luehr
Associate Professor of Mathematics

This dissertation was submitted to the Graduate Faculty of the College of Engineering and to the Graduate Council, and was accepted as partial fulfillment of the requirements for the degree of Doctor of Philosophy.

August 1979

Herbert A. Bevis
Dean, College of Engineering

Dean, Graduate School